SANDIA REPORT

SAND97–0590 • UC–410
Unlimited Release
Printed March 1997

Final Report on LDRD Project: Artificial Atoms

J. A. Simmons, T. M. Eiles, J. S. Moon, J. R. Wendt, J. F. Klem, J. Reno

Prepared by
Sandia National Laboratories
Albuquerque, New Mexico 87185 and Livermore, California 94550

Sandia is a multiprogram laboratory operated by Sandia Corporation, a Lockheed Martin Company, for the United States Department of Energy under Contract DE-AC04-94AL85000.

Sandia National Laboratories

Issued by Sandia National Laboratories, operated for the United States Department of Energy by Sandia Corporation.

Available to DOE and DOE contractors from
Office of Scientific and Technical Information
P.O. Box 62
Oak Ridge, TN 37831

Prices available from (615) 576-8401, FTS 626-8401

Available to the public from
National Technical Information Service
U.S. Department of Commerce
5285 Port Royal Rd
Springfield, VA 22161

NTIS price codes
Printed copy: A04
Microfiche copy: A01

SAND97-0590
Unlimited Release
Printed March 1997

Distribution
Category UC-410

Final Report on LDRD Project: Artificial Atoms

J. A. Simmons, T. M. Eiles, J. S. Moon
Nanostructure and Semiconductor Physics Department

J. R. Wendt, J. F. Klem
Compound Semiconductor Materials and Processes Department

J. Reno
Semiconductor Material and Device Sciences Department

Abstract

This project involves the fabrication and study of novel semiconductor nanostructures sufficiently small that the electronic energy states are confined in all three dimensions, and are thus 0-dimensional. They contain only a handful of electrons, and are therefore similar to individual atoms, but artificially made. With sensitive measuring techniques at millikelvin temperatures, the individual electrons in can be observed and controlled. Two types of artificial atoms (AAs) were investigated: (1) capacitive AAs, quantum dots linked to an electron reservoir by tunnel barriers, and (2) resonant tunneling AAs, quantum antidots around which electrons are magnetically bound. Because at high magnetic fields 2D electrons must travel in 1D "edge states" along the boundary of the sample, we also investigated edge states to determine if they can exhibit self-interference when sufficiently small. Our research has focused on (1) growing ultra high purity GaAs material for AAs, (2) developing low-noise cryogenic measurement circuitry using an in-situ HEMT transistor, itself at temperatures below 1K, (3) capacitive measurements of edge states in high magnetic fields (4) fabrication of gate-defined sub-micron capacitive AAs in fractional quantum Hall effect materials, (5) measurements of electron focusing around large arrays of antidots, and (6) measurements of the edge state propogation direction in the fractional quantum Hall effect regime.

Intentionally Left Blank

Table of Contents

Intentionally Left Blank

Final Report on LDRD Project: Artificial Atoms

Case Number: 3539.440

Project Manager: S. T. Picraux, 1112

Principal Investigators: J. A. Simmons, 1112, J. S. Moon, 1112, J. R. Wendt, 1311, J. F. Klem, 1311, J. L. Reno, 1113

Abstract

This project involves the fabrication and study of novel semiconductor nanostructures sufficiently small that the electronic energy states are confined in all three dimensions, and are thus 0-dimensional. They contain only a handful of electrons, and are therefore similar to individual atoms, but artificially made. With sensitive measuring techniques at millikelvin temperatures, the individual electrons in can be observed and controlled. Two types of artificial atoms (AAs) were investigated: (1) capacitive AAs, quantum dots linked to an electron reservoir by tunnel barriers, and (2) resonant tunneling AAs, quantum antidots around which electrons are magnetically bound. Because at high magnetic fields 2D electrons must travel in 1D "edge states" along the boundary of the sample, we also investigated edge states to determine if they can exhibit self-interference when sufficiently small. Our research has focused on (1) growing ultra high purity GaAs material for AAs, (2) developing low-noise cryogenic measurement circuitry using an in-situ HEMT transistor, itself at temperatures below 1K, (3) capacitive measurements of edge states in high magnetic fields (4) fabrication of gate-defined sub-micron capacitive AAs in fractional quantum Hall effect materials, (5) measurements of electron focusing around large arrays of antidots, and (6) measurements of the edge state propogation direction in the fractional quantum Hall effect regime.

Accomplishments

The project goal is deeper understanding of the basic science of electrons in confined nanostructures. The fabrication and measurement of nanostructures containing only a few electrons is challenging, and required developing several novel steps in growth, fabrication, and quantum-limited measurement . We achieved the following milestones: (1) Used molecular beam epitaxy to grow ultra-pure high mobility GaAs material for artificial atoms (Aas), acheiving new Sandia records for ultra-high mobilities of 3.6 x 106 cm2/Vs at densities sufficiently low the the fractional quantum Hall effect can be reached. . (2) We developed two sensitive measurement circuits for detecting capacitance. One technique uses an in-situ high electron mobility transistor (HEMT) located within the cryostat and kept at a temperature of less than 1K. Because the transistor is cold, it not only acts as a capacitance buffer, but also has exceptionally low noise. We were able to measure capacitance to a resolution of 30 attofarads. (3) We also fabricated and tested an ultra-sensitive, quantum-limited electron detector, the Coulomb blockade electrometer (CBE), for detecting individual electrons in the AAs. This enabled us to clearly observe

individual electrons moving within this device at a temperature of 280 mK. (See Fig. 1.) (4) Integrated the CBE electron detector with a quantum dot AA of diameter < 1 micron, manufactured in high mobility material. (See Fig. 2.) (5) Fabricated and measured resonant tunneling AAs in high purity material, developing a new electron beam lithography technique. The channels on either side of the quantum antidot had their conductances quantized in the fundamental units $2e^2/h$, indicating that electrons traversed them ballistically, without any scattering. When both channels were measured together, the conductance was quantized in units of $4e^2/h$, indicating a quantum coherence between them. (6) Using the artificial atom described in (5), we performed the world's first observation of magnetic focusing around a single quantum antidot. When only one channel was open, a monotonic magneto-resistance (MR) was observed. However, when both channels were open, large MR peaks appeared due to electrons being magnetically focused from one channel, around the antidot, and into the other channel. Accordingly, the conductance of both channels was NOT equal to the sum of the conductances of each channel, a violation of Ohm's law. Second-order MR peaks also appeared, due to a specular reflection of electrons off the center antidot. As the antidot size is tuned via gate bias, the field position of the MR peaks shifts. A simple theoretical model of the shift is consistent with other measured parameters. (7) Perhaps our most significant result, we were able to demonstrate by capacitive measurements that edge state transport breaks down not only at low magnetic fields, as expected, but also for special values of high magnetic fields where each electron is associated with an even number of magnetic flux quanta. At these special values of magnetic field, new particles are formed called composite fermions, which behave like electrons at zero magnetic field. The ability to measure the breakdown is expected to provide important information on the properties of composite fermions, currently an exciting research topic at the forefront of basic condensed matter physics. (8) Large arrays of etched quantum antidots exhibited focusing phenomenon both for electrons near zero magnetic field, and for composite fermions near special values of magnetic field (even number of flux quanta for each electron.) This data, once analysis is complete, should also provide important information on the properties of composite fermions.

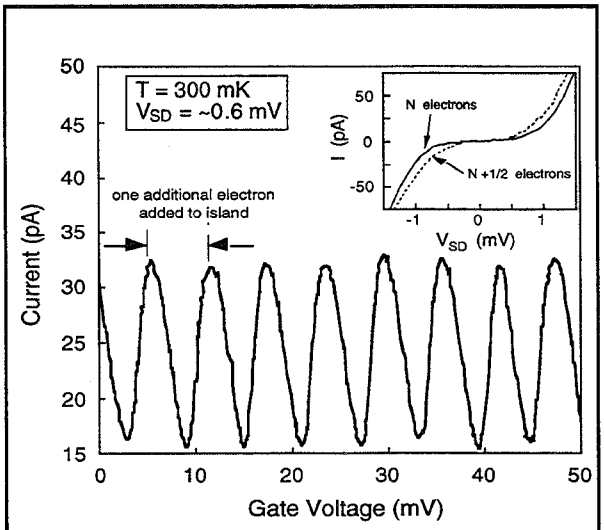

FIG. 1. Current through CBE vs. gate voltage, with source-drain voltage fixed at ~0.6 mV. Each peak corresponds to adding a single electron to the island. Inset: current vs. source-drain voltage for two gate biases corresponding to integer and half-integer electron occupancy.

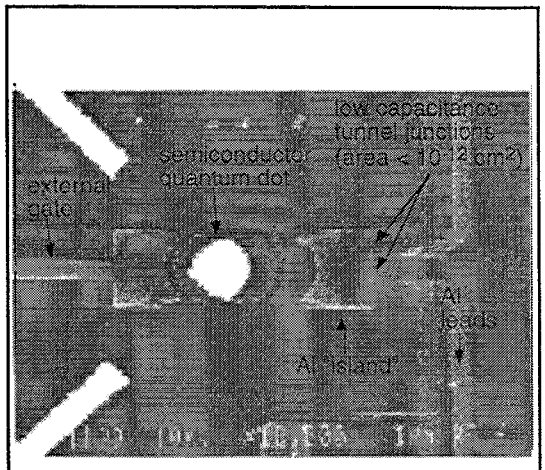

FIG. 2. Electron micrograph of Coulomb Blockade device, appearing to right of the photo. It is shown integrated with a nearby semiconductor quantum dot of ~0.7 micron diameter, in the center of the photo.

List of Publications and Presentations

Publications

1. M. E. Sherwin, J. A. Simmons, T. M. Eiles, N. E. Harff, and J. F. Klem, "Parallel quantum point contacts fabricated with independently biased gates and a submicrometer airbridge post," *Applied Physics Letters* **65**, 2326-2328 (31 October, 1994).

2. T. M. Eiles, J. A. Simmons, M. E. Sherwin, and J. F. Klem, "Magnetic focusing in parallel quantum point contacts," *Physical Review B* **52**, 10756-10759, (15 October, 1995).

3. H. C. Chui, B. E. Hammons, N. E. Harff, J. A. Simmons, and M. E. Sherwin, "2 x 10^6 cm^2/Vs electron mobility by metalorganic chemical vapor deposition with tertiarybutylarsine," *Applied Physics Letters* **68**, 208-210, (8 January, 1996).

4. J. A. Simmons, R. R. Du, M. A. Zudov, H. C. Chui, N. E. Harff, and B. E. Hammons, "Composite Fermions in 10^6 cm^2/Vs Mobility AlGaAs/GaAs Heterostructures Grown by MOCVD," in *Proceedings of the 23rd International Conf. on the Physics of Semiconductors,* edited by M. Scheffler and R. Zimmermann. Singapore: World Scientific, Vol. 3, 1996, pgs. 2511-2514.

5. J. A. Simmons, M. E. Sherwin, M. V. Weckwerth, N. E. Harff, T. M. Eiles, W. E. Baca, H. Hou, and B. E. Hammons, "Advanced Fabrication Technologies for Nano-Electronics," in *Proceedings of the 24th State-of-the-Art Program on Compound Semiconductors*, edited by Ren, F, and S. Pearton, S. Chu, R. Shul, W. Pletschen, and T. Kamijoh. Pennington, New Jersey: The Electrochemical Society, Vol. 96-2, 1996, pgs. 186-202.

Presentations

1. M. E. Sherwin, J. A. Simmons, J. C. Zolper, and J. F. Klem, "Advanced fabrication of mesoscopic devices in AlGaAs/GaAs," Advanced Heterostructure Workshop, Kona, Hawaii, December 4-9, 1994.

2. T. M. Eiles, J. A. Simmons, M. E. Sherwin, and J. F. Klem, "Magnetic focusing in parallel quantum point contacts," American Physical Society March Meeting, 23 March 1995, San Jose, California.

3. H. C. Chui, B. E. Hammons, N. E. Harff, J. A. Simmons, and M. E. Sherwin, "2 x 10^6 cm^2/Vs Electron Mobility By MOCVD With Tertiarybutylarsine," 37th Electronic Materials Conference, 21 June 1995, Charlottesville, Virginia.

4. J. A. Simmons, H. C. Chui, N. E. Harff, B. E. Hammons, H. Q. Hou, R. R. Du, and M. A. Zudov, "MOCVD Growth Of GaAs/AlGaAs Heterostructures For Fractional Quantum Hall Effect Studies," American Physical Society March Meeting, 18 March 1996, St. Louis, Missouri.

5. M. A. Zudov, R. R. Du, J. A. Simmons, and H. C. Chui, "Electron And Composite Fermion Transport In MOCVD-Grown GaAs/AlGaAs Heterostructures," American Physical Society March Meeting, 18 March 1996, St. Louis, Missouri.

6. J. A. Simmons, R. R. Du, M. A. Zudov, H. C. Chui, N. E. Harff, and B. E. Hammons, "Composite Fermions in 2 x 106 cm2/Vs Mobility AlGaAs/GaAs Heterostructures Grown by MOCVD," 23rd International Conf. on the Physics of Semiconductors, 21 July 1996, Berlin, Germany

7. J. A. Simmons, M. E. Sherwin, M. V. Weckwerth, N. E. Harff, T. M. Eiles, W. E. Baca, H. Hou, and B. E. Hammons, "Advanced Fabrication Technologies for Nano-Electronics," State-of-the-Art Program on Compound Semiconductors XXIV, 6 May 1996, Los Angeles, California.

Parallel quantum point contacts fabricated with independently biased gates and a submicrometer airbridge post

M. E. Sherwin, J. A. Simmons, T. E. Eiles, N. E. Harff, and J. F. Klem
Center for Compound Semiconductor Technology, Sandia National Laboratories, Albuquerque, New Mexico 87185-0603

(Received 27 June 1994; accepted for publication 26 August 1994)

Using an integrated airbridge and submicrometer gate post technology, coupled quantum point contacts (QPCs) arranged in a parallel configuration were fabricated. The airbridge and gate post are fabricated by e-beam lithography and Ti/Au evaporation in a single step. Gate post diameters as small as 0.1 μm have been achieved. The two QPCs are fabricated with two conventional gates and a central airbridged gate, each of which can be biased independently. Conductance measurements clearly exhibit coupling of the two QPCs, as the quantized conductance steps are in units of 4 e^2/h. Independent measurements of each QPC show conductance steps in units of 2 e^2/h.

The fabrication of mesoscopic devices has recently been advanced through improvements in backgating technology[1,2] and independently tunable submicrometer gates.[3,4] These advanced fabrication techniques will enable the fabrication of new quantum devices. We have developed an integrated airbridge and submicrometer gate post for use in surface Schottky gates that can be independently biased. The airbridge and gate post are fabricated in a single step and are easily incorporated into existing processes. In this letter we demonstrate the application of the integrated airbridge/gate post to the fabrication of parallel coupled quantum point contacts.

Recent efforts at submicrometer gating by Taylor[3] and Simpson[4] have focused on the use of an interlevel dielectric to act as a spacer between multiple metal levels. However, the addition of a dielectric spacer adds two processing steps to the fabrication sequence and generally requires dry etching of the dielectric. The plasma processing associated with both dielectric deposition and etch can have a significant deleterious impact on the device.[5] Taylor and Simpson have designed their processes with a first level metal disk to protect the semiconductor from plasma damage during the dry etching of the dielectric. Since the contact hole through the dielectric must line up with the first level metal disk, this places stringent limitations on the minimum size of the metal disk.

An attractive alternative fabrication process is the use of self-supporting metallic airbridges with submicrometer gate posts.[6] In this letter we describe the fabrication of metallic airbridges with spans approaching 20 μm and gate posts with contact diameters down to 0.1 μm. Following the normal first level metallization, the airbridge process requires one electron-beam lithography step followed by a single metal evaporation and lift-off. The final structure leaves the semiconductor surface free of dielectric overlayers and there is no need for a potentially damaging dry etch. We have applied our process to the fabrication of a split-gate quantum point contact structure[7] with three independently biased contacts. The two outer gates are conventional first level metal and the central gate is a submicrometer post dropped from the airbridge. Although to date we have applied the airbridge/gate post process only to this type of structure, we believe that it will have great utility in the fabrication of additional nanostructures such as Coulomb blockade devices, quantum dots, and gate-defined arrays of quantum wires.

The material used in this work was an MBE-grown $Al_{0.3}Ga_{0.7}As/GaAs$ heterostructure with the 2DEG located ~1200 Å beneath the surface. A 250 Å donor layer Si-doped to 1×10^{18} cm^{-3} was separated from the 2DEG by a 400 Å $Al_{0.3}Ga_{0.7}As$ spacer layer. The 2DEG has a density of 2.0×10^{11} cm^{-2} with a mobility of 10^6 cm^2/V s, without illumination. Optically defined Hall bars were fabricated by wet etching. Large area Au/Ge/Ni contacts and Cr/Au gate leads were optically defined and deposited by lift-off. The two outer first level gates of the device are then patterned by e-beam lithography and a Cr/Au lift-off.

After the first level gate metallization is complete, the airbridge formation is begun by spinning a bilayer resist profile of 600 nm of PMMA (496 K) followed by 1200 nm of P(MMA-MAA) 9%. The P(MMA-MAA) layer is spun on in two coatings of equal thickness. After each spin the sample is hot plate baked at 180 °C for 15 min. The e-beam exposure of the airbridge structure requires a number of different doses for the different regions of the device, as listed in Table I. A high dose exposes both resist layers to define the large area support pillars and lines. Lower doses expose only the P(MMA-MAA) layer to define the actual bridge region, though because of differing electron backscatter rates this dose depends on whether the bridge crosses a GaAs surface or first level metal. A third, higher dose is used to define the submicrometer gate post. We also make use of a transition

TABLE I. Exposure doses for the airbridge definition. The difference between the bridging doses over GaAs and Au is a result of increased backscatter of the electron beam over the Au gates. The transition dose is used between lines on GaAs and bridges over GaAs.

Exposure region	Dose (uC/cm^2)
2 μm wide lines on GaAs	320
2 μm wide bridges over GaAs	160
2 μm wide bridges over Au	140
Transition dose (line bridge)	250
0.2 μm square gate post	400[a]

[a]This dose results in a contact diameter of 0.25 μm on the GaAs substrate.

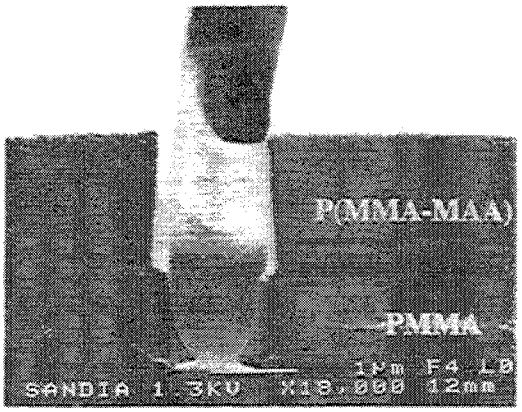

FIG. 1. Resist profile of PMMA and P(MMA-MAA) bilayer after electron-beam exposure and development in MIBK:IPA (1:2). The actual resist thicknesses in this sample are larger than that quoted in the letter. Au sputtering was used to reduce charging effects during inspection, which resulted in the clear contrast between the two resist layers.

dose between a bridging region and the large support pillars. The e-beam lithography system was operated at 50 keV with a beam current of 2 nA. The airbridge is 2.0 μm wide and the contact hole is drawn as a 0.2 μm square hole in the center of the airbridge. After exposure, the sample is developed in MIBK:IPA (1:2) at room temperature for 3 min with light agitation. Figure 1 shows an example of the developed resist profile for a similar airbridge structure clearly showing the ability to selectively open holes to the substrate while maintaining a bridge above the bottom layer of resist. The P(MMA-MAA) layer shows excellent undercut which allows a clean lift-off profile. Although it is possible to use a trilevel resist profile, we have found that the bilayer resist is more than adequate for good lift-off. The bottom PMMA layer acts to guide the metal bridge over various topography, including etched facets and first level metal. We have found that the airbridge can span topography that is as tall as the bottom PMMA layer thickness.

Following the resist development, the sample is descumed and dipped in buffered oxide etch before loading into the evaporator. For this resist profile a Ti/Au (50/650 nm) metallization is defined by lift-off in acetone. We have previously reported on the fabrication of taller bridging structures with larger dimensions.[6] The process has a good amount of latitude and can be engineered for different applications. In the present application the airbridge is ~0.5 μm above the semiconductor surface and the gate post has a controllable minimum of 0.1 μm. If the airbridge is lowered so that it is closer to the substrate then it should be possible to fabricate gate posts with even smaller diameters. Figure 2 shows the completed structure with first level gates and the airbridge. Varying the dose from 380 to 440 uC/cm^2 increases the gate post diameter from 0.1 to 0.45 μm.

A similar airbridge approach, albeit for larger critical dimensions, has been previously reported[8] but this technique relies on the use of a complex development sequence for each layer of the trilayer resist profile. Other techniques have required multiple e-beam exposures and metal evaporations.[9] Our technique uses a single exposure, a single development

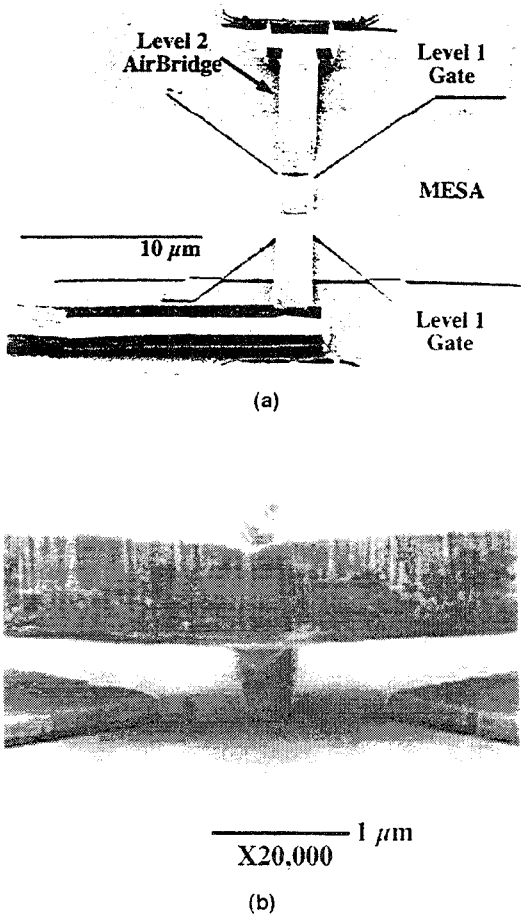

FIG. 2. Final device structure for the parallel quantized conductance channels. The side gates are first level metal (Cr/Au), and the center gate post and airbridge are second level metal (Ti/Au). The exposure conditions used are listed in Table I. (a) Low magnification overview image with the different regions labeled. The white arrow indicates the point of view for (b). The actual structure shown is not one that was electrically measured.

followed by a single metal evaporation and lift-off, with the advantage that the minimum feature size is not limited by alignment considerations.

The conductance through the parallel QPCs formed on either side of the gate post was measured at 40 mK using standard low-frequency lock-in techniques. Depletion under the gates occurred at -0.25 V. The gap between either side gate and the center gate post is approximately 0.7 μm. Figure 3 shows the quantized conductance steps for two conditions: (a) all three gates swept together, and (b) with one QPC fully pinched off by a side and center voltage of -5.5 V and the other side gate swept. No gate leakage was measured at any time during the measurements. When one QPC was fully depleted [Fig. 3(b)], the quantized conductance step heights from the second quantum point contact were 2 e^2/h. When both quantum point contacts were open [Fig. 3(a)], the quantized conductance step heights were 4 e^2/h. Steps of 4 e^2/h were observed when all three gates were swept together or when the center gate was swept with the side gates held at a constant bias. The locking of both quantum point contacts together into conductance steps of 4 e^2/h was explained with a minimum-energy argument by Smith

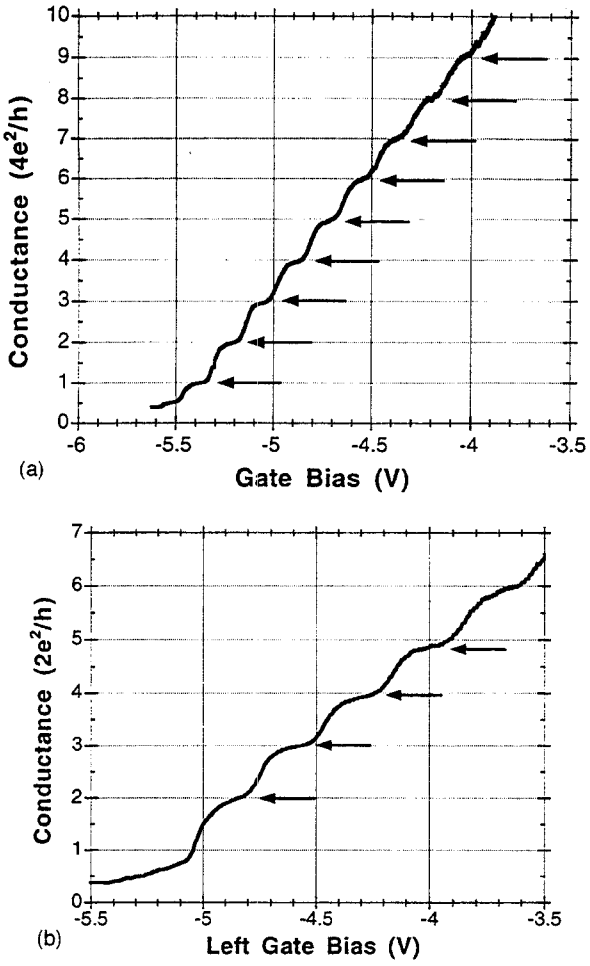

FIG. 3. Quantized conductance steps for the structure in Fig. 2. (a) All three gates were swept together. The quantized conductance steps are in units of 4 e^2/h. (b) Same structure with the right side QPC fully pinched off. The left side gate was swept from -5.5 to -3.5 V. The quantized conductance steps are in units of 2 e^2/h.

et al.[10] When the two QPCs are within the electron phase coherence length, the QPCs form a coupled system and the subbands depopulate together. The QPC metallurgical width was quite large in this sample and a high gate bias of ~ -5.5 V was needed to pinch off the channels, with the result that the effective channel length was quite long due to the shape of the charge depletion profile. This had the effect of degrading the quality of the quantized conductance steps. Additionally, the two QPCs pinched off at different biases (-5.5 and -5.0 V) when operated independently. SEM inspection of similar devices have shown excellent alignment of the center gate post in the middle of the two side gates, so we are forced to attribute the pinch off bias difference to random potential fluctuations in the channels.

One concern about the fabrication process relates to the possibility of electron-beam damage to the underlying heterostructure beneath the airbridge. To address this issue we exposed a multisegmented Hall bar to various electron-beam currents and doses at 50 keV and remeasured the mobilities at 0.3 K. We observed no variation of the mobility as a function of electron-beam current or dose. This is in contrast to the data of Ghanbari,[11] but is in agreement with the more recent work of Tanaka.[12] The maximum electron-beam energy that Tanaka explored was 25 keV, but his arguments should still be valid for 50 keV e-beam exposure.

In summary, we have presented a technique for the fabrication of ≥ 0.1 μm diameter gate posts with integrated airbridges for use in three-dimensional wiring or mesoscopic device fabrication. Successful application of our technique to the observation of parallel quantized conductance channels has been demonstrated, and the technique should be able to be extended to even smaller dimensions.

We would like to thank Ted Castillo for his assistance during device fabrication. This work was performed at Sandia National Laboratories in the Compound Semiconductor Research Laboratory and was supported by the Department of Energy under Contract No. DE-AC04-94AL85000.

[1] K. M. Brown, E. H. Linfield, D. A. Ritchie, G. A. C. Jones, M. P. Grimshaw, and M. Pepper, Appl. Phys. Lett. **64**, 1827 (1994).
[2] M. E. Sherwin, J. A. Simmons, J. F. Klem, and J. C. Zolper (unpublished).
[3] R. P. Taylor, J. A. Adams, M. Davies, P. A. Marshall, and R. Barber, J. Vac. Sci. Technol. B **11**, 628 (1993).
[4] P. J. Simpson, C. J. B. Ford, D. R. Mace, I. Zailer, M. Yosefin, M. Pepper, J. T. Nicholls, D. A. Ritchie, J. E. F. Frost, M. P. Grimshaw, and G. A. C. Jones, Surf. Sci. **305**, 453 (1994).
[5] A. J. Murrell, R. C. Grimwood, P. O'Sullivan, M. Gilbert, K. Vanner, F. Ruddell, I. Davies, K. Hilton, S. Bland, and D. Spear, Proceedings of the GaAs IC Symposium, 1992 (unpublished), p. 173.
[6] M. E. Sherwin, R. Corless, and J. R. Wendt, J. Vac. Sci. Technol. B **11**, 339 (1993).
[7] J. A. Simmons, S. W. Hwang, D. C. Tsui, and M. Shayegan, Superlatt. Microstruct. **11**, 223 (1992).
[8] A. Ketterson, M. Tong, J.-W. Seo, K. Nummila, K. Y. Cheng, J. Morikuni, S. Kang, and I. Adesida, J. Vac. Sci. Technol. B **10**, 2936 (1992).
[9] R. G. Woodham, R. M. Jones, D. G. Hasko, J. R. A. Cleaver, and H. Ahmed, Microelectron. Eng. **17**, 563 (1992).
[10] C. G. Smith, M. Pepper, R. Newbury, H. Ahmed, D. G. Hasko, D. C. Peacock, J. E. F. Frost, D. A. Ritchie, G. A. C. Jones, and G. Hill, J. Phys. Condens. Matter **1**, 6763 (1989).
[11] R. A. Ghanbari, M. Burkhardt, D. A. Antoniadis, H. I. Smith, M. R. Melloch, K. W. Rhee, and M. C. Peckerar, J. Vac. Sci. Technol. B **10**, 2890 (1992).
[12] N. Tanaka and T. Ishikawa, J. Electron. Mater. **23**, 341 (1994).

Intentionally Left Blank

Magnetic focusing in parallel quantum point contacts

T.M. Eiles, J.A. Simmons, M.E. Sherwin, and J.F. Klem
Sandia National Laboratories, Albuquerque, NM 87185

Using a novel air-bridged gate, we have fabricated two closely spaced parallel quantum point contacts (QPCs) in a GaAs-AlGaAs heterostructure. By biasing the gates appropriately, we have measured the magnetoresistance (MR) at low fields for both single and parallel point contacts. Assuming a parabolic potential, the MR of a single QPC can be quantitatively understood by a previous theory incorporating magnetic field-suppressed backscattering. However, the MR of two QPCs in parallel displays resistance peaks, implying a failure of Ohm's law due to coupling between the channels. These resistance peaks are shown to be due to magnetic focusing of electrons from one channel into the other.

"Ballistic" electron transport can occur within devices smaller than the electron mean free path, and is a particularly simple regime in which to study electron coherence phenomena. The simplest ballistic device is the quantum point contact (QPC), a narrow constriction patterned in a two dimensional electron gas (2DEG) whose width is on the order of the Fermi wavelength and whose length is shorter than the mean free path, so that it must be treated as an electron wave guide supporting a number of lateral one-dimensional modes. Several experimental configurations have exhibited such coherence phenomena as quantized conductance and electron beam collimation.[1] However, semiclassical arguments not involving the wave nature of electronic motion can be used to interpret much of the data. For example, the magnetoresistance (MR) of a single QPC was interpreted by a semiclassical theory to adduce various features of the QPC's potential profile. In addition, magnetic focusing, a classical effect, has been observed in devices in which QPCs inject and collect electrons moving in cyclotron orbits.[2]

In this paper we discuss magnetotransport measurements of a system of two closely spaced parallel QPCs separated by a tunable potential maximum, or "antidot," created by an independently biased center gate (Fig. 1). This system has been used to study resonant tunneling between edge states in the high-field quantum Hall regime,[3] and also the parallel addition of QPC conductances at zero field.[4] We focus in this work, however, on the semiclassical ballistic regime at low magnetic fields. Though the low field MR data for single constrictions are well described by present theory, we find that the data for two parallel QPCs depart significantly from Ohm's law. MR peaks are found corresponding to a focusing of electron paths from one constriction to the other around the center antidot gate. While earlier work did find structure in the MR related to classical cyclotron orbits, the structures were either two dimensional antidot arrays[5] or linear arrays of multiple closely spaced QPCs fabricated by focused ion beams[6] and therefore did not allow the antidot potential to be tuned independently of the adjacent QPC parameters, nor the individual QPCs to be characterized. Here we present MR focusing data, taken over a broad range of gate bias parameters, for a single tunable antidot bounded by two independently tunable and well characterized QPCs. This enables us to observe the evolution of MR peaks with changing antidot potential which is found to be consistent with independent measurements of the gate-induced edge depletion.

We fabricated the samples from two standard GaAs heterostructures: sample A with mobility μ = 800,000 cm^2/Vs and two-dimensional electron density n_{2D} = 1.2 x 10^{11} cm^{-2} and sample B with μ = 10^6 cm^2/Vs and n_{2D} = 2.0 x 10^{11} cm^{-2}. The center gate (0.3 μm diameter) drops from an air bridge suspended over both side gates, allowing

separate bias voltages V_i (i = 1-3) to be applied to each of the gates. Fabrication details have been published elsewhere.[7] ac Current (0.3 to 3 nA) is driven through the device, and the bulk Hall resistance R_H and the four-terminal longitudinal resistance R_L are measured by a low-frequency lock-in technique.

In Fig. 2 we show the low field four-terminal magnetoresistance of a single point contact for a series of gate voltages. In our measurements of conductance vs. gate voltage at $B = 0$, only during a fraction of temperature cyclings were we able to observe well-defined steps. This is probably due to backscattering from impurities or dopant potentials in the fairly long (> 0.5 μm) constrictions formed by the gate depletion.[8] The MR is characteristically negative at the lowest fields, becoming positive at a crossover point B_c. The resistance drop at the lowest fields was observed by van Houten *et al*, and was explained in terms of suppressed backscattering due to localization of the electron cyclotron orbits near the sample walls.[9] This behavior can be understood quantitatively by the four-terminal resistance formula:

$$R_L = \frac{h}{2e^2}\left(\frac{1}{N_{pc}(B)} - \frac{1}{N_{bulk}(B)}\right) \qquad (1)$$

Both the number of transmitting bulk channels $N_{bulk} = (h/2e)n_{2D}/B$ and the number of channels in the point contact $N_{pc}(B)$ can be treated as continuous classical variables in the low-field regime we discuss here. The evolution of the number of channels in the constriction with B depends on the nature of the confinement potential, and has been calculated for both hard wall and parabolic confinement potentials. Simulations of narrow split gate point contacts yield potentials which are more-or-less flat-bottomed in the case of wide constrictions, but which evolve into more parabolic shapes as the constriction is narrowed.[10]

For a hard wall potential, the number of channels in the constriction does not vary much if $B < B_c$, so the (negative) slope of the MR is basically the same as that of the Hall resistance ($1/en_{2D}$). Because the crossover field B_c increases as the point contact width is decreased, the magnitude of the resistance drop increases with negative bias. In contrast to previous work, our data do not demonstrate this trend; in fact, the net drop in resistance decreases slightly as the QPC is closed. The solution to this discrepancy is in a more accurate modeling of the QPC as a parabolic potential. We find that all our curves are best fit by the parabolic confinement model. In this model, the important parameters are the one-dimensional electron density n_{1D} and the characteristic frequency of the parabolic potential Ω. The number of populated channels is given by

$$N_{pc}(B) = \left[\frac{3\pi}{4} n_{1D} \sqrt{\frac{\hbar}{2m^*\Omega}}\right]^{2/3} \frac{1}{\sqrt{\left(1+(\alpha B)^2\right)}} \qquad (2)$$

where $\alpha = e/m^*\Omega$.[11] The solid lines in Fig. 2 are fits to eqn. (1) using the measured bulk n_{2D}, and with n_{1D} and Ω as fitting parameters.

It is possible[11] to define an effective QPC width

$$W_{eff} = \frac{n_{1D}}{n_{2D}^{QPC}} \qquad (3)$$

using the 2D density in the constriction n_{2D}^{QPC}. Following Berggren *et al*, we compare eqn. (2) in the high-field ($\alpha B \gg 1$) limit with the filling factor in the constriction written in terms of the two-dimensional density: $N_{pc} = (h/2e) n_{2D}^{QPC}/B$. Comparing equations (2) and (3) yields the effective width:

$$W_{eff} = 2\pi n_{1D}^{1/3} \left(\frac{2\hbar}{3\pi m^*\Omega}\right)^{2/3} \qquad (4)$$

In the inset we show a plot of the calculated effective width derived from the fitting parameters as a function of the gate voltage applied. The dependence is linear, with the result that the width decreases by about 0.2 μm/V with the applied voltage, in good agreement with the depletion data. Recently, several theories have predicted various approaches to understanding the potential profile,[12] and we suggest that MR measurements may play a future role in better understanding the point contact potential.

In Fig. 3 we show low-field MR data for *two* parallel point contacts for a series of different center gate voltages with the outer gate voltages held constant, so that both contacts are being narrowed simultaneously as the area of the center antidot is increased. Instead of the smooth MR curve of the single point contact, resistance peaks appear at low magnetic fields ($B < 100$ mT). The peaks do not appear at all unless there is depletion under the center gate (data from second-to-lowest curve), which divides the channel into two separate QPCs. They begin to disappear again as the constrictions are made very narrow (data not shown). The peak positions do not change appreciably as a function of the center gate voltage. They are symmetric in magnetic field, and not part of a periodic oscillation, making it doubtful that their origin is due to quantum interference. They also persist to $T = 4$ K. These peaks are a clear departure from Ohm's law, which would combine the MR curves for two parallel QPCs, yielding a smooth MR with the

same shape as the single QPC MR. As such, the peaks must be due to coupling between the conduction channels in the two QPCs. MR peaks related to trapped cyclotron orbits have been reported in antidot arrays and the resistance peaks we see are reminiscent of these.[5] Using $k_F = (2\pi n_{2D})^{1/2}$ and the measured peak position of 60 mT, we find a cyclotron radius $R_c = \hbar k_F/eB = 0.8$ μm, which is consistent with the lithographic dimensions and the smooth parabolic potential indicated by our data from a single QPC. The constancy of the peak position for all gate voltages seems surprising, at least when the constriction potential is thought of as bounded by hard walls which move laterally as the split gates deplete the 2DEG. However, as seen in the single channel data, the low density of our samples yields a parabolic potential which gradually rises up to the Fermi level as the gate voltage is increased. The electrons are thus mostly emitted from the center of the constriction which remains at a fairly constant position.

The above discussion can be quantified by first observing exactly how Ohm's law for combining the two resistances is circumvented in this geometry. This was done by taking MR curves for the parallel QPC configuration, then pinching off the two point contacts in succession and measuring the two individual single QPC MR scans. In Fig. 4 we show the magnetoconductance (MC) for three bias conditions. The large dots are the MC for the parallel case, displaying the conductance dip corresponding to the focused orbit. The lines are the sum of the conductances for the constituent point contacts. A small offset was added to make the curves coincide at $B = 0$; this accounts for the unavoidable effect that pinching off one side of the device has on the other side. The double QPC conductance drops at low fields, and then follows the shape of the single QPC combination, though there is a fairly constant conductance deficit which persists to higher B. The data indicate that at fields well below the focusing peak, the two QPCs allow independent electron transport.

Further evidence of electron focusing can be seen in the data plotted in Fig. 5, where the side gates have been carefully balanced to give each of the constrictions the same width. Another set of peaks lies beyond the primary focusing peaks, becoming more prominent as the QPCs are narrowed. In contrast to the primary focusing peak, the position of these secondary peaks decreases substantially with negative center gate voltage. This secondary peak is suggestive of a magnetically focused trajectory similar to those seen in other experiments where electrons reflect specularly off a potential barrier.[2] Here, the secondary peak is due to the orbit in which the electron makes a single reflection off the antidot potential [see inset]. The sharpness of the secondary peaks is dependent on the degree to which electrons are emitted directly out of the QPC, known as collimation, as well as to the degree to which reflection is specular as opposed to diffuse.

Normally, collimation is best accomplished when the width of the QPC is narrower, on the order of the Fermi wavelength. This is consistent with the increasing sharpness of the secondary peaks as the constrictions are narrowed.[1] As discussed previously, increasing the antidot voltage does not affect the primary peak position much because the electrons are chiefly emitted from the QPC center. However, the effective diameter of the potential antidot induced by the center gate increases with negative bias, so the focusing radius required to make a single reflection from this potential decreases.

We can quantify the behavior of the antidot potential by plotting the ratio of the primary peak position to the secondary peak potential as a function of antidot voltage, shown in the inset to Fig. 3. Since this ratio is also that of the secondary cyclotron radius R_{c2} to the primary radius R_c, we can fit it to a simple model of the geometry of the system which assumes collimated electron emission, a single specular reflection from the antidot potential, and a linear relationship between the effective antidot radius d and the applied voltage: $R_{c2}/R_c = 0.5[1+(d/R_c)^2]$. The fit to the data yields $d/R_c = 0.25|V-V_{dep}|$ with V in volts (V_{dep} = -0.6 V is the depletion voltage); that is, d changes by 0.2 μm for every volt applied to the antidot (R_c = 0.8 μm), which is in good agreement with what we find in the conductance vs. voltage dependence. Orbits consisting of additional reflections could not be observed, but the secondary peaks are further evidence of focusing in this system.

In conclusion, marked deviations from Ohm's law have been observed in the low field magnetoresistance of closely spaced parallel QPCs. Though the low field data for a single point contact can be closely matched to previously existing theory, the coupled system has transport features which cannot be explained by it. Rather, the features are consistent with cyclotron orbits reminiscent of those seen in antidot arrays. This is a demonstration of how transport anomalies related to classical focusing trajectories can be seen in a system consisting of a single antidot.

We acknowledge a helpful conversation with S. Goodnick. This work was supported by the U.S. DOE under Contract No. DE-AC04-94AL85000.

References

1. For a review, see H. van Houten, C.W.J. Beenacker, and B.J. van Wees, in *Semiconductors and Semimetals*, ed. by M.A. Reed (Academic, New York, 1989).

2. H. van Houten *et al*, Phys. Rev. B **39**, 8556 (1989).

3. J.A. Simmons *et al*, Phys. Rev. Lett. **63**, 1731 (1989); P.J. Simpson, *et al*, Surf. Sci. (1994); C.J.B. Ford *et al*, J. Phys.: Condens. Matter **6**, L725 (1994).

4. C.G. Smith *et al*, J. Phys.: Condens. Matter **1**, 6765 (1989): S.W. Hwang, J.A. Simmons, D.C. Tsui, and M. Shayegan, Phys. Rev. B **44**, 13497 (1991).

5. D. Weiss *et al*, Phys. Rev. Lett. **66**, 2790 (1991).

6. K. Nakamura *et al*, Appl. Phys. Lett. **56**, 385 (1990); Y. Hirayama and T. Saku, Phys. Rev. B **42**, 11408 (1990).

7. M.E. Sherwin, J.A. Simmons, T.M. Eiles, N.E. Harff, and J.F. Klem, Appl. Phys. Lett. **65**, 2326 (1994).

8. J.A. Nixon, J.H. Davies, and H.U. Baranger, Phys. Rev. B **43**, 12638 (1991). The backscattering could be made worse by the relatively low density and corresponding poor screening in our samples.

9. H. van Houten *et al*, Phys. Rev. B **37**, 8534 (1988).

10. S.E. Laux, D.J. Frank, and Frank Stern, Surf. Sci. **196**, 101 (1988).

11. K.-F. Berggren, G. Roos, and H. van Houten, Phys. Rev. B **37**, 10118 (1988).

12. I.E. Aronov, M. Jonson, and A.M. Jagoskin, Phys. Rev. B **50**, 4590 (1994).

Figure Captions

1. SEM photograph of the airbridge structure and split gates used to define the two point contacts. Numbered voltages are applied to the gates as indicated. The lithographic width of the 2DEG channels on either side of the center gate is 0.8 μm.

2. Series of low-field magnetoresistance scans (sample B) for a single quantum point contact taken at $T = 0.3$ K (thick lines). Voltages applied [in volts] were: $V_1 = -3.2$, $V_2 = -2.7$, and $V_3 = -0.5, -0.75, -1.0, -1.2, -1.3, -1.4, -1.5$, and -1.6. Thin lines are fits to eqn. 1 assuming a parabolic potential for the point contact. Inset: Effective channel width as a function of gate voltage, obtained using the characteristic frequency and the 1-D density parameters obtained in the fits.

3. Resistance vs. magnetic field curves for parallel point contacts in sample A. The side gates were set at $V_1 = V_3 = -0.8$ V, and the center gate voltage was stepped at V_2 [in volts] = 0, -0.5, -0.9, -1.4, -1.6, -1.8, -1.9, -2.1, -2.3, -2.4, and -2.5.

4. Low-field magnetoconductance scans at three bias conditions of the two QPCs of sample B measured in parallel (dots), along with the *sum* of the conductances of the two QPCs measured individually (solid line).

5. Magnetoresistance of parallel point contacts (sample A) with optimized balance between both point contacts, taken at $T = 0.3$ K. Side gate voltages [in volts] were $V_1 = -0.7$, $V_3 = -0.9$, and the center gate voltages were = -1.6, -2.0, -2.2, -2.35, -2.45, -2.50, and -2.55 V. Curves are offset on the resistance axis to accentuate the secondary reflection peaks (marked by dots) appearing on the shoulders of the primary focusing peaks. Inset: ratio of secondary to primary peak position as a function of center gate voltage. The solid line is the quadratic fit discussed in the text.

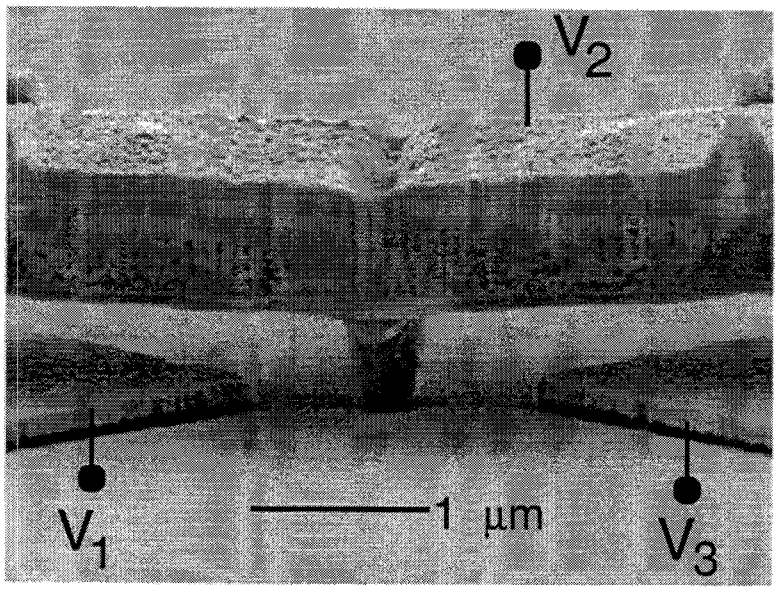

FIG. 1

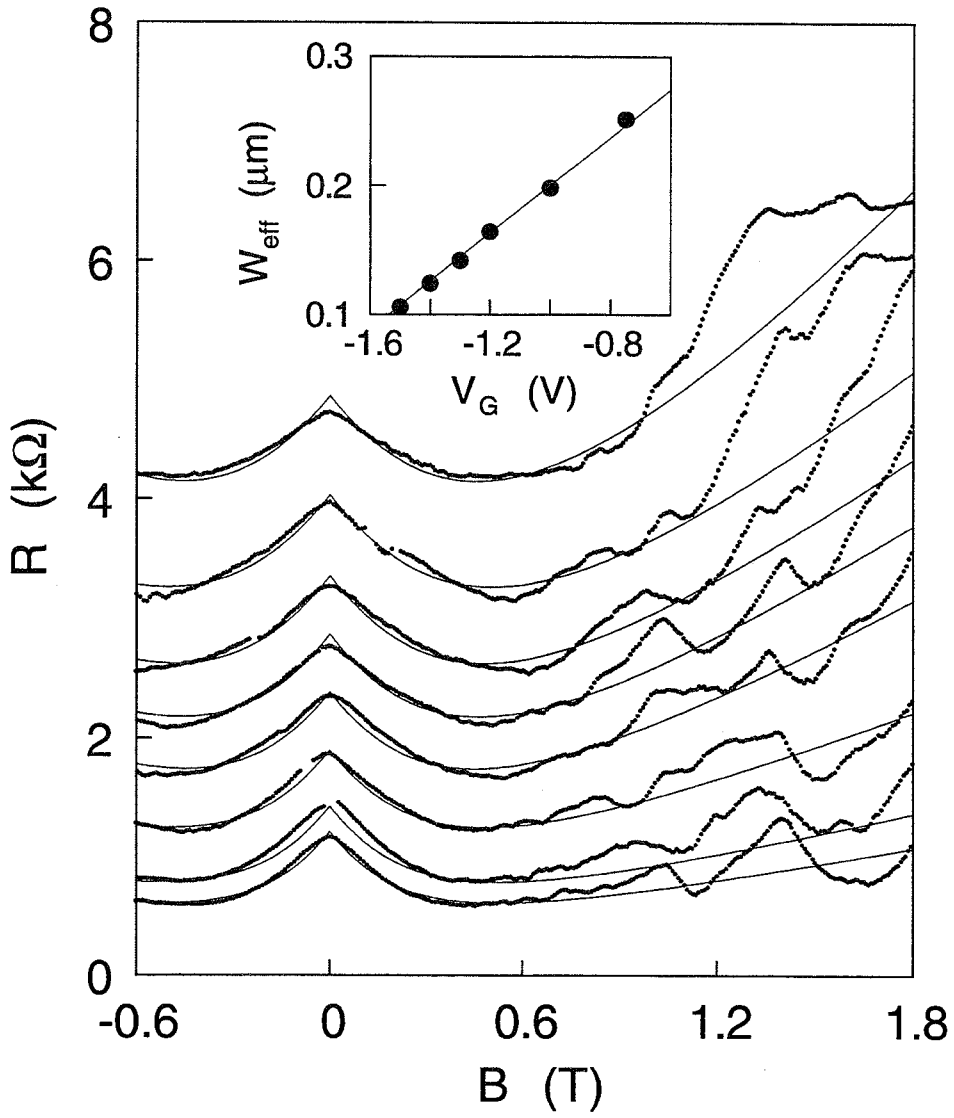

FIG. 2

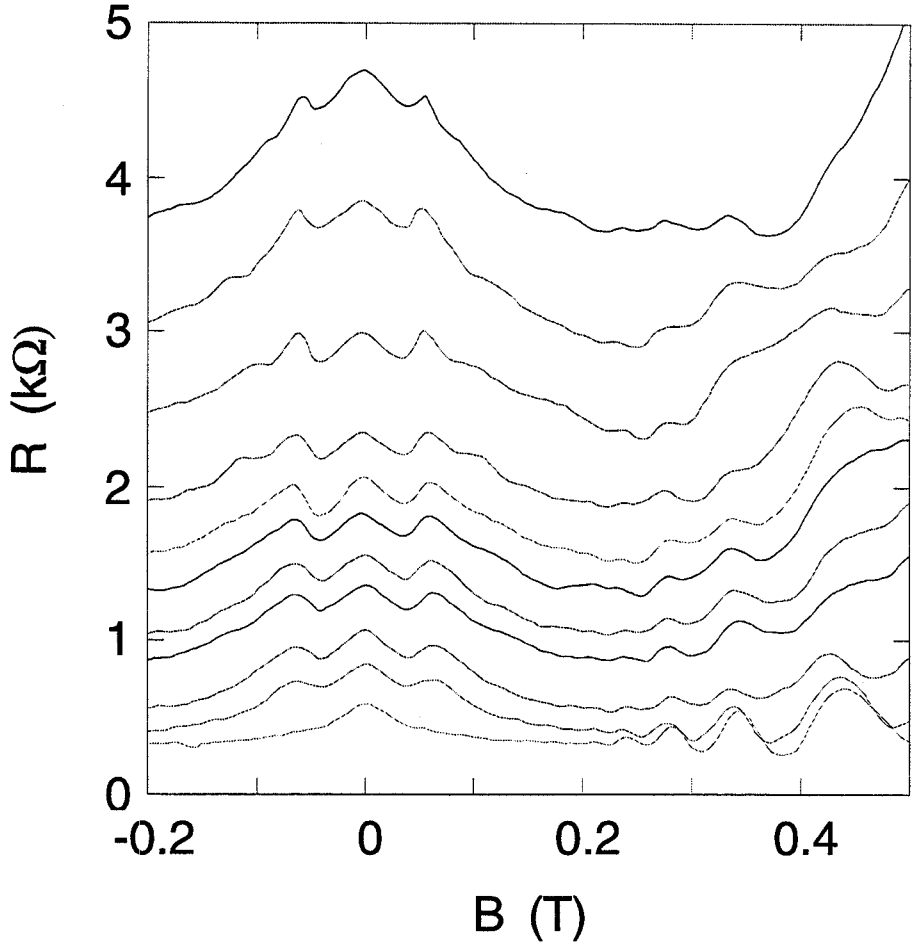

FIG. 3

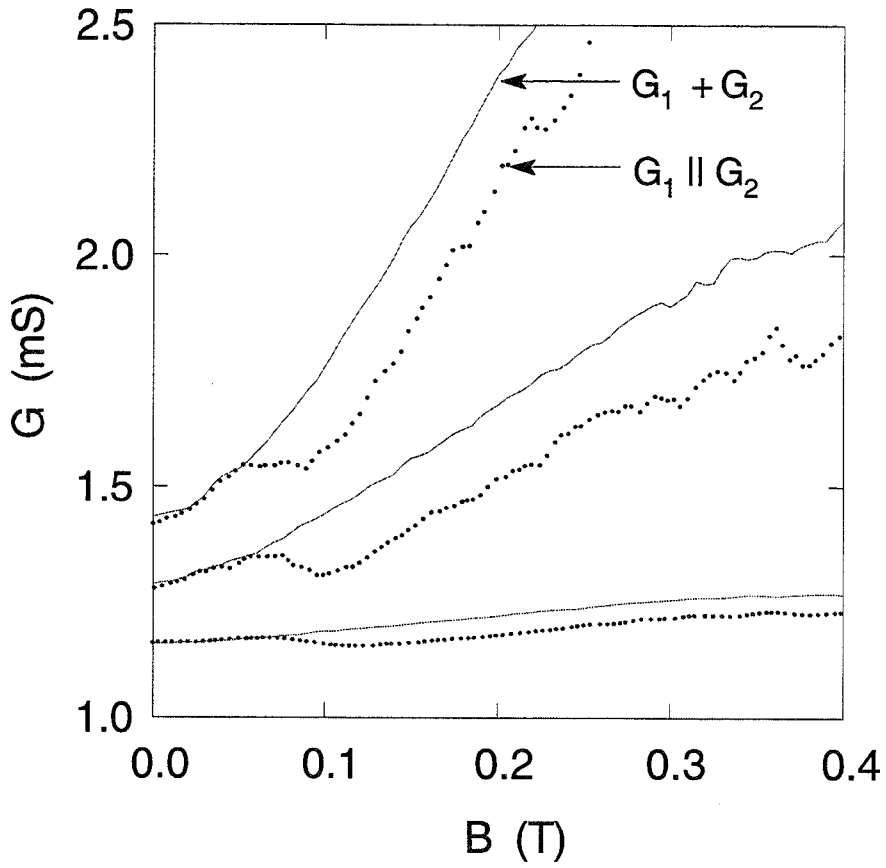
2.5
2.0
1.5
1.0
G (mS)
0.0
0.1
0.2
0.3
0.4
B (T)
G1 + G2
G1 || G2

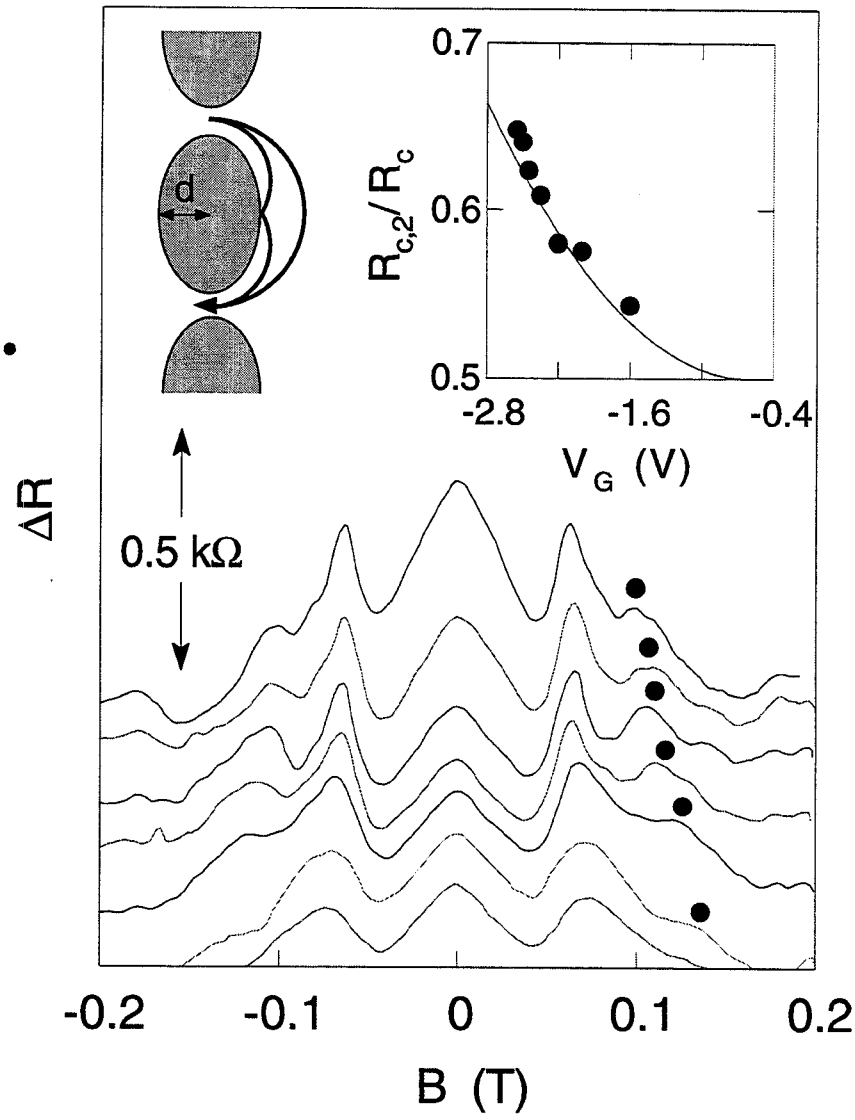

FIG. 5

Intentionally Left Blank

2×10^6 cm^2/V s electron mobility by metalorganic chemical vapor deposition with tertiarybutylarsine

H. C. Chui,[a] B. E. Hammons, N. E. Harff, J. A. Simmons, and M. E. Sherwin
Sandia National Laboratories, Albuquerque, New Mexico 87185-0603

(Received 10 July 1995; accepted for publication 26 October 1995)

We demonstrate the metalorganic chemical vapor deposition (MOCVD) growth of two-dimensional electron gases (2DEGs) with electron mobilities up to 2.0×10^6 cm^2/V s at 0.3 K. These are the highest mobilities to date for MOCVD materials, and were achieved using a safer replacement precursor for arsine, tertiarybutylarsine (TBA). For structures grown using arsine, we obtained a maximum mobility of 1.0×10^6 cm^2/V s, which although comparable to the best by MOCVD to date, is half that obtained using TBA. Our studies on thick GaAs and AlGaAs layers indicate that the use of TBA in place of arsine reduces both the carbon and donor impurity concentrations. Thus, TBA is not only a safe alternative to arsine, but also produces significantly purer films. © *1996 American Institute of Physics.* [S0003-6951(96)01502-3]

Metalorganic chemical vapor deposition (MOCVD) for the growth of III–V semiconductors has been a rapidly developing technology over the past decade with continuing improvements in reactor design and precursor purity. As compared to molecular beam epitaxy (MBE), MOCVD has advantages including high quality regrowth, ability to rapidly and continuously vary alloy compositions, and low defect densities. Most importantly, MOCVD is recognized as a key technology for manufacturing due to its high throughput, short downtimes, and scalability to large reactors. However, there are two primary disadvantages of MOCVD: lower material purity compared to MBE, and safety concerns due to highly toxic arsine gas. Tertiarybutylarsine (TBA) is a low pressure, less toxic liquid that is highly promising as a safe replacement precursor for arsine. To date, there has been concern about the purity of material grown with the carbon-containing TBA, despite reports that films grown with TBA can be comparable to, if not slightly purer than, films grown with arsine.[1–6]

In this letter, we demonstrate that TBA can produce significantly purer films than arsine. We use AlGaAs/GaAs two-dimensional electron gases (2DEGs) as an ultimate test of material purity, since the low temperature mobility of 2DEGs is extremely sensitive to background impurities.[7] We first describe the optimization of 2DEG growth using arsine. We then present results on 2DEGs grown using TBA that exhibit mobilities up to 2.0×10^6 cm^2/V s. These are the highest mobilities to date for MOCVD materials[8–12] and approach state-of-the-art MBE mobilities.[13–17] Finally, results from thick GaAs and AlGaAs layers grown with arsine and TBA are used to explain the higher mobilities of TBA 2DEGs.

The samples were grown in a high purity Emcore reactor as described previously.[11] For bulk GaAs layers grown with arsine, we obtained mobilities of 160 000 cm^2/V s at 77 K, comparable to the best to date at 77 K. For 2DEG studies, the basic epitaxial structure consisted of 1 μm undoped GaAs, an undoped $Al_{0.28}Ga_{0.72}As$ spacer of varying thickness, a $\sim4\times10^{12}$ cm^{-2} Si delta-doping layer, 625 Å undoped $Al_{0.28}Ga_{0.72}As$, and a 50 Å GaAs cap. Quantum Hall measurements were performed with a standard lock-in technique at 0.3 K as described previosuly.[11] We emphasize that unlike previous reports,[8,10] our measurement technique ensured that there was no parallel conduction path to the 2DEG channel in any of the data presented here, since the minima in the longitudinal resistance ρ_{xx} closely approached zero for small integer Landau level filling factors ν.

In our previous work with arsine, we demonstrated 2DEGs with mobilities up to $\mu=7.9\times10^5$ cm^2/V s for a low electron density of $n=3.0\times10^{11}$cm^{-2} at 0.3 K.[11] These 2DEGs had the highest mobility figure of merit $\mu/n^{3/2}$ to date[13,14] and exhibited the fractional quantum Hall effect (FQHE)[18] for the first time in MOCVD material. In this letter, we have further optimized the mobilities of 2DEGs grown with arsine by varying the V/III ratio and spacer thickness. We first investigated the effect of V/III ratio on 2DEG mobility. Samples were grown with varying V/III ratios of 190, 144, and 98, a constant spacer thickness of 400 Å, and a uniformly doped 250 Å AlGaAs doping layer instead of delta doping.[11] The mobilities of the three samples were similar ($\sim6\times10^5$ cm^2/V s after illumination), implying that the V/III ratio had little effect on arsine 2DEG mobility over the range of V/III ratios studied. With this range of V/III ratios, bulk GaAs with arsine varied from light p type to n type. The spacer thickness dependence of 2DEG mobility and carrier density was also characterized. Shown in Fig. 1(a) is the dependence of mobility on spacer thickness as measured in the dark and after illumination at 0.3 K. The spacer thickness was varied from 200 to 525 Å with a constant delta-doping density and a V/III ratio of 190. The arsine 2DEGs had a peak mobility of 1.0×10^6 cm^2/V s for a carrier density of 4.6×10^{11} cm^{-2} at a spacer thickness of 300 Å. With smaller spacers, the mobility decreased due to increased ionized impurity scattering from the Si modulation doping layer. At larger spacers, the mobility was nearly con-

[a]Present address: Hewlett Packard, 370 West Trimble Road, MS 91 UJ, San Jose, CA 95131.

 0003-6951/96/68(2)/208/3/$6.00

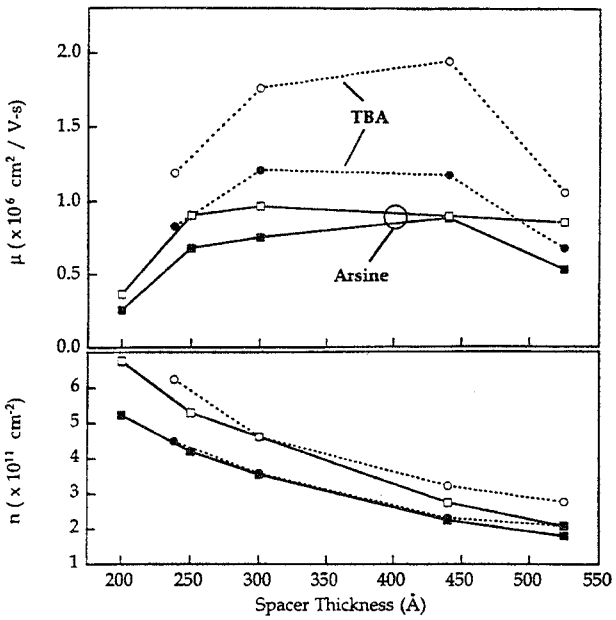

FIG. 1. Mobility [top graph: 1(a)] and carrier density [bottom graph: 1(b)] dependence on spacer thickness for 2DEGs grown with arsine (squares and solid lines) and TBA (circles and dashed lines). Samples were measured at 0.3 K in the dark (solid markers) and after illumination (hollow markers).

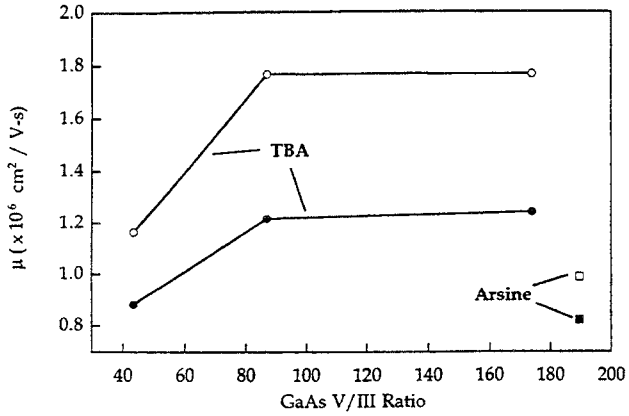

FIG. 2. Mobility dependence on V/III ratio for 2DEGs grown with arsine (squares) and TBA (circles). Samples were measured at 0.3 K in the dark (solid markers) and after illumination (hollow markers).

stant and only decreased slightly due to a decreasing carrier density[7] as shown in Fig. 1(b).

For growth using TBA, we first investigated the effect of V/III ratio on the 2DEG mobility. These 2DEGs had a spacer thickness of 300 Å and a V/III ratio ranging from 43 to 174. Shown in Fig. 2 is the dependence of mobility on V/III ratio for these 2DEGs. We observed an increase in mobility as the V/III was increased from 43 to 87, probably due to a decrease in carbon concentration in the epilayers. At a higher V/III of 174, the mobility remained the same as the V/III of a 87 sample, probably since the carbon concentration was reduced to a level where it was no longer the limiting scattering source. At the higher V/III ratios, the 2DEGs had a mobility of 1.8×10^6 cm^2/V s after illumination at 0.3 K. For comparison, we also grew an identical 2DEG sample with arsine at a V/III ratio of 190; the mobility of the arsine sample was 1.0×10^6 cm^2/V s after illumination, significantly lower than the TBA mobilities.

We also investigated the dependence of TBA 2DEG mobility on spacer thickness. These samples had a moderate V/III ratio of 87 and a spacer thickness ranging from 238 to 525 Å. The dark and light mobilities at 0.3 K for these samples are plotted in Fig. 1 together with mobilities of arsine-grown samples. The mobility of the TBA samples depend in the same manner on spacer thickness as the arsine samples. The mobility peaked at a spacer thickness of 440 Å with larger and smaller spacers yielding lower mobilities due to decreased carrier density and increased impurity scattering, respectively. The carrier density dependence on spacer thickness is also shown in Fig. 1(b) and follows closely that of the arsine samples. The peak mobility at a spacer thickness of 440 Å was 2.0×10^6 cm^2/V s, the highest mobility achieved to date by MOCVD.[8–12] The corresponding 2DEG density was only 3.2×10^{11} cm^{-2}, significantly lower than densities of previous MOCVD high mobility samples, so that the mobility figure of merit [13,14] ($\mu/n^{3/2}$) for this sample was 1.1×10^{-11} cm^5/V s, almost twice that of previously reported 2DEGs grown with arsine.[8–11] This sample had dark mobilities (carrier concentrations) at 300, 77, and 0.3 K of 6500 (4.1×10^{11}), 1.8×10^5 (2.8×10^{11}), and 1.2×10^6 cm^2/V s (2.3×10^{11} cm^{-2}), respectively. As a comparison with previous MOCVD high mobility results, in Fig. 3 we have plotted low temperature mobility as a function of carrier density for the best MOCVD samples to date. Our arsine 2DEGs are comparable to the best reported to date, implying that the purity of our arsine and reactor are excellent. Even so, our TBA 2DEGs have significantly higher mobilities than all of the previous results based on arsine. We used several batches of arsine over the course of our study, thereby verifying that the lower arsine mobilities are not due to the particular arsine batch. We also note that, although the previously reported mobilities were at temperatures from 1.5 to 4.2 K,[8–12] the mobility is essentially independent of temperature for temperatures below ~5 K and mobilities below $\sim2\times10^6$ cm^2/V s.[7,11,16,17] With these extremely high mobility samples, we observed the FQHE with very sharp features, indicative of very high quality material. Shown in Fig. 4 is the longitudinal resistance as a function of magnetic field at 0.3 K for the 525 Å spacer TBA sample that has a mobility of 1.1×10^6 cm^2/V s at a carrier density of 2.9×10^{11} cm^{-2}. Sharp minima in the longitudinal resistance as a function of magnetic field can be seen at fractional filling factors of $\frac{4}{5}$, $\frac{5}{5}$, $\frac{7}{5}$, and $\frac{8}{5}$ in a progression towards $\frac{3}{2}$.[18] These features are much sharper than observed with arsine samples.[11] The longitudinal resistance also approaches zero at integral filling factors, implying that there are no parallel conduction paths to the 2DEG. With a better optimized doping and layer structure, even higher mobilities can probably be achieved with TBA.

In order to understand the higher mobilities of TBA grown 2DEGs compared to arsine 2DEGs, we have examined thick GaAs and AlGaAs grown with TBA and arsine. With arsine, 8 μm thick GaAs layers were grown with vary-

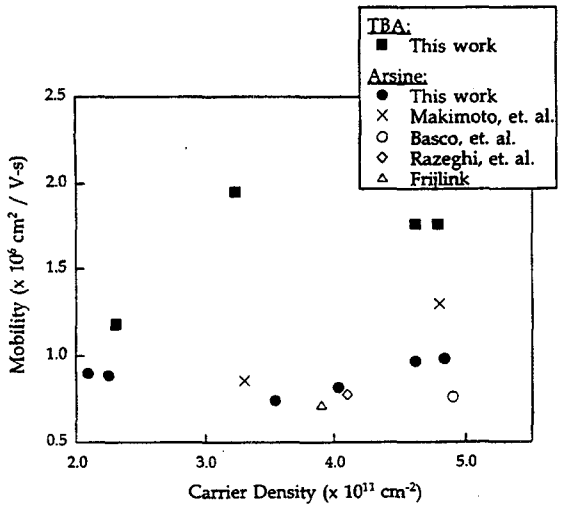

FIG. 3. Mobility vs carrier density for the highest mobility 2DEGs grown by MOCVD to date.

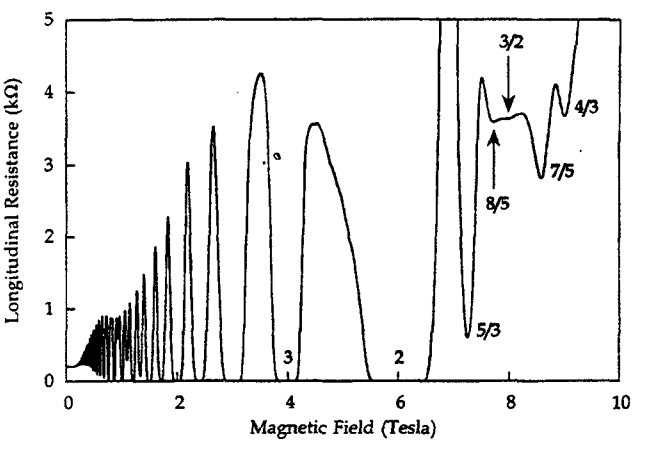

FIG. 4. Longitudinal resistance vs magnetic field for a 2DEG sample grown with TBA measured at 0.3 K. Sharp minima were observed at fractional filling factors of $\frac{4}{3}$, $\frac{5}{3}$, $\frac{7}{5}$, and $\frac{8}{5}$ in a progression towards $\frac{3}{2}$.

ing V/III ratio from 40 to 150. The GaAs changed from p type to n type as the V/III ratio was increased to above ~60. Near the crossover point, the carrier concentration was as low as $n=2\times10^{14}$ cm^{-3}, while at high V/III ratios, $n\sim1\times10^{15}$ cm^{-3}. Other groups have attributed this behavior to a reduction in carbon incorporation with increasing V/III ratio leaving an n-type background.[1,19] This n-type background has been reported to be Ge or Si from germane or silane impurities in the arsine.[19–22] For 8 μm GaAs layers grown with TBA covering V/III from 5 to 120, all samples were p type with decreasing carrier concentration down to $<2\times10^{14}$ cm^{-3} for increasing V/III ratio. The reduction in p-type concentration with increasing V/III was similarly due to a reduction in carbon incorporation.[1] However, since the GaAs remained p type even at high TBA V/III ratios, the donor impurity concentration was very low compared to arsine samples.[2] A similar behavior was observed for $Al_{0.25}Ga_{0.75}As$ grown with arsine and TBA. n-type AlGaAs was obtained with arsine at a V/III of 200, while TBA AlGaAs remained p type at all V/III ratios studied.[4] Low temperature photoluminescence measurements showed that AlGaAs grown with TBA had a lower carbon concentration than arsine AlGaAs for similar V/III ratios.[4] We also note that high purity GaAs and AlGaAs grown by MBE are p type, as we find with TBA materials.

In conclusion, we have demonstrated the highest mobility MOCVD material to date with mobilities up to 2.0×10^6 cm^2/V s by using TBA as a replacement for arsine. With arsine, we have obtained a maximum mobility of 1.0×10^6 cm^2/V s comparable to the best MOCVD mobilities to date, but only half that of TBA 2DEGs. By studying thick GaAs and AlGaAs layers, we find that the use of TBA in place of arsine reduces both the carbon and donor impurity concentrations, resulting in 2DEG mobilities that even by MBE are quite difficult to obtain. Thus, with the advantages of both safety and purity, TBA may well become the standard arsenic precursor thereby eliminating the primary advantages of MBE compared to MOCVD.

The authors acknowledge J. Y. Tsao, S. T. Picraux, and T. E. Zipperian for continued support. This work is funded by U. S. Department of Energy Contract No. DE-AC04-94AL85000.

[1] S. P. Watkins and G. Haacke, Appl. Phys. Lett. **59**, 2263 (1991).
[2] S. P. Watkins, D. M. Brake, and G. Haacke, J. Appl. Phys. **75**, 2952 (1994).
[3] T. Kikkawa, H. Tanaka, and J. Komeno, J. Appl. Phys. **67**, 7576 (1990).
[4] R. M. Biefeld, H. C. Chui, B. E. Hammons, W. G. Breiland, T. M. Brennan, E. D. Jones, M. H. Kim, P. Grodzinski, and H. C. Lee (unpublished).
[5] H. C. Chui, R. M. Biefeld, B. E. Hammons, W. G. Breiland, T. M. Brennan, E. D. Jones, M. H. Kim, P. Grodzinski, K. H. Chang, and H. C. Lee (unpublished).
[6] J. A. Baumann, C. Michel, H. Marek, H. B. Serreze, and R. Schachter, J. Electron. Mater. **19**, 363 (1990).
[7] W. Walukiewicz, H. E. Ruda, J. Lagowski, and H. C. Gatos, Phys. Rev. B **30**, 4571 (1984).
[8] T. Makimoto and N. Kobayashi, Jpn. J. Appl. Phys. **32**, 648 (1993).
[9] M. Razeghi, M. Defour, F. Omnes, M. Dobers, J. P. Vieren, and Y. Guldner, Appl. Phys. Lett. **55**, 457 (1989).
[10] R. Basco, F. Agahi, and K. M. Lau, Appl. Phys. Lett. **63**, 1960 (1993).
[11] H. C. Chui, B. E. Hammons, J. A. Simmons, N. E. Harff, and M. E. Sherwin, Appl. Phys. Lett. **67**, 1911 (1995).
[12] P. M. Frijlink, J. Cryst. Growth **93**, 207 (1988).
[13] J. H. English, A. C. Gossard, H. L. Störmer, and K. W. Baldwin, Appl. Phys. Lett. **50**, 1826 (1987).
[14] M. Shayegan, V. J. Goldman, C. Jiang, T. Sajoto, and M. Santos, Appl. Phys. Lett. **52**, 1086 (1988).
[15] C. T. Foxon, J. J. Harris, D. Hilton, J. Hewett, and C. Roberts, Semicond. Sci. Technol. **4**, 582 (1989).
[16] L. N. Pfeiffer, K. W. West, H. L. Stormer, and K. W. Baldwin, Appl. Phys. Lett. **55**, 1888 (1989).
[17] T. Saku, Y. Hirayama, and Y. Horikoshi, Jpn. J. Appl. Phys. **30**, 902 (1991).
[18] D. C. Tsui and H. L. Stormer, IEEE J. Quantum Electron. **QE-22**, 1711 (1986).
[19] M. H. Kim, S. S. Bose, B. J. Skromme, B. Lee, and G. E. Stillman, J. Electron. Mater. **20**, 671 (1991).
[20] M. Hata, N. Fukuhara, Y. Zempo, M. Isemura, T. Yako, and T. Maeda, J. Cryst. Growth **93**, 543 (1988).
[21] S. P. Watkins and G. Haacke, J. Appl. Phys. **69**, 1625 (1991).
[22] S. Holmes, C. C. Phillips, R. A. Stradling, Z. Wasilewski, R. Droopad, S. D. Parker, W. T. Yuen, P. Balk, A. Brauers, H. Heinecke, C. Plass, M. Weyers, C. T. Foxon, B. A. Joyce, G. W. Smith, and C. R. Whitehouse, Semicond. Sci. Technol. **4**, 782 (1989).

Intentionally Left Blank

COMPOSITE FERMIONS IN 2 x 10^6 cm^2/Vs MOBILITY AlGaAs/GaAs HETEROSTRUCTURES GROWN BY MOCVD

J. A. SIMMONS[a], R. R. DU[b], M. A. ZUDOV[b],
H. C. CHUI[a], N. E. HARFF[a] and B. E. HAMMONS[a]
[a] *Sandia National Laboratories, P. O. Box 5800, Albuquerque, NM 87185 USA*
[b] *Dept. of Physics, Univ. of Utah, Salt Lake City, UT 84112 USA*

ABSTRACT

We report on our recent growth by MOCVD of 2.0 x 106 cm2/Vs mobility heterostructures. These mobilities, the highest reported to date, are attributed to the use of tertiarybutylarsine as the arsenic precursor. Measurements in tilted magnetic fields of the FQHE states near filling factor 3/2 are consistent with a spin-split composite fermion (CF) model proposed earlier. The extracted values of the product of the CF g-factor and CF effective mass agree with values previously obtained for MBE samples.

As compared to molecular beam epitaxy (MBE), metalorganic chemical vapor deposition (MOCVD) has several advantages including high quality regrowth, easily variable alloy compositions, low defect densities, and superior uniformity. However, until recently MOCVD growth has had two serious disadvantages: (1) safety concerns due to the use of highly toxic arsine gas, and (2) considerably lower material purity. The latter has meant that MOCVD-grown two dimensional electron gases (2DEGs) were too low in mobility to allow observation of the fractional quantum Hall effect (FQHE), which is easily destroyed by disorder. Because MOCVD material parameters such as impurity potential profile, defect density, uniformity, and interface quality, are possibly different from in MBE, it is worthwhile to examine the behavior of the FQHE in MOCVD material.

In this paper we report on our recent MOCVD growth[1] of high quality 2DEGs with mobilities as high as 2.0 x 10^6 cm^2/Vs at a density of 3.2 x 10^{11} cm^{-2}. These mobilities were acheived using low-toxicity tertiarybutlyarsine (TBA) as the arsenic precursor, instead of arsine. The use of TBA results in roughly a factor of two improvement in mobility. Using this material, we also studied the FQHE states near Landau level (LL) filling factor $\nu = 3/2$ in tilted magnetic fields. The data is consistent with the same spin-split composite fermion (CF) proposed earlier for MBE material by Du et al.[2] Using this model, we measure the product of the CF effective g-factor g^* and the CF effective mass m_{CF}. After taking into account the expected square root dependence[3] of m_{CF} on the external perpendicular magnetic field $B_\perp$, the measured values of $g^* m_{CF}$ for our MOCVD material are found to be in agreement with those previously obtained[2] for MBE.

The heterostructures were grown in an Emcore reactor described previously,[4] and consisted of 1 μm of undoped GaAs, an undoped $Al_{0.28}Ga_{0.72}As$ spacer of varying thickness, a ~4 x 10^{12} cm^{-2} Si delta-doping layer, 625 Å of undoped $Al_{0.28}Ga_{0.72}As$, and a 50 Å GaAs cap. Samples using both arsine and TBA as the arsenic precursor were

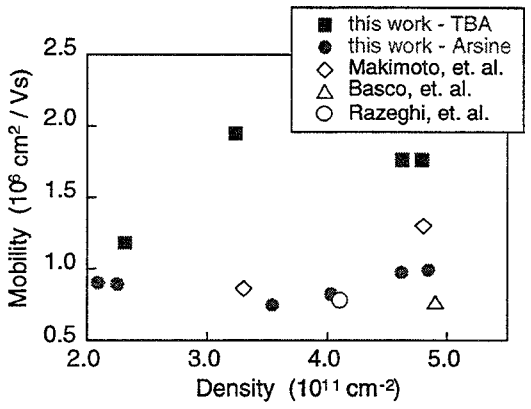

FIG. 1. Highest MOCVD mobilities to date.

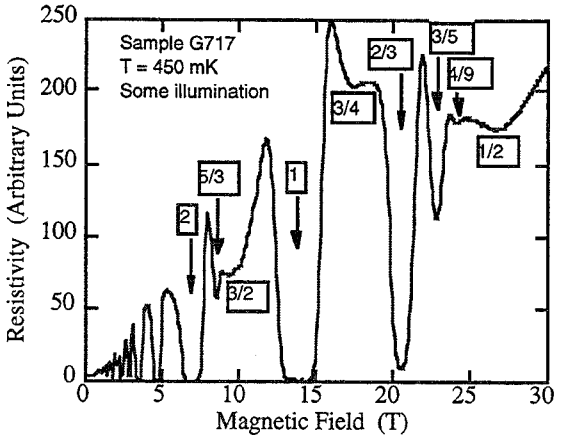

FIG. 2. R_{xx} of the 2 x 10^6 cm^2/Vs sample at 0.45 K.

grown. Mobility and density were measured via a standard lock-in technique at 0.3 K. As described elsewhere,[1] variation of the V/III ratio for arsine-grown 2DEGs caused little change in 2DEG mobility, and a cross-over in undoped bulk GaAs from p-type to n-type with increasing V/III ratios. However, for TBA-grown 2DEGs, the mobility increased for V/III ratios up to ~90, after which it leveled off, and undoped bulk GaAs remained weakly p-type for all V/III ratios measured, up to ~150. We attribute this behavior to a reduced incorporation of Si and Ge n-type impurites with the use of TBA, since typically these impurities arise from trace amounts of silane and germane in the arsine.[5] Accordingly, TBA-grown 2DEGs exhibited significantly higher mobilities and higher quality FQHE states than those grown with arsine. In Fig. 1 we plot mobility vs. density for the best MOCVD samples grown to date. While our arsine mobilities are comparable to those acheived by others,[6] our TBA 2DEGs have mobilities almost double those of all previous results based on arsine. Fig. 2 shows the longitudinal magnetoresistance R_{xx} of our highest mobility (2.0 x 10^6 cm^2/Vs) sample, at 450 mK. The FQHE states are quite strong for this temperature, and exhibit a rather low Dingle temperature of ~4 K.

In a similar TBA sample with density 2.8 x 10^{11} cm^{-2}, we studied the FQHE states around ν=3/2 in a total magnetic field B_{TOT} applied at an angle θ from normal. The sample was measured in the dark at 50 mK. Fig. 3 shows R_{xx} vs. perpendicular field $B_\perp$ between ν=1 and ν=2 for several θ, with the positions of the $\nu=(3p\pm2)/(2p\pm1)$ FQHE states indicated. As θ is increased, the minima associated with these ν disappear and then reappear. For example, 4/3 exhibits a strong minimum at 0°, which evolves into a maximum at 38.1°, and again becomes a minimum for θ>47°. Similar oscillatory behavior is observed for 7/5, 8/5, and 11/7. However, 5/3 remains a strong minimum for all θ.

The data can be understood in terms of the spin-split CF model of Du et al.[2] This model is similar to the standard CF model,[3] in that electrons at a $B_\perp$ such that ν is near 3/2 are treated as new particles, CFs, subject to an *effective magnetic field* $B_\perp^* = 3(B_\perp - B_\perp^{3/2})$. The FQHE of electrons near 3/2 can then be viewed as an integer QHE of the CFs due to the the effective field $B_\perp^*$. The energy spacing between the CF "Landau levels"

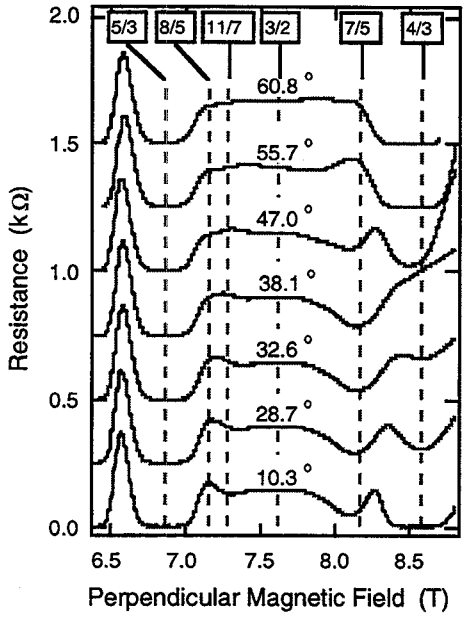

FIG. 3. R_{xx} vs. perpendicular magnetic field $B_\perp$ for several different tilt angles θ.

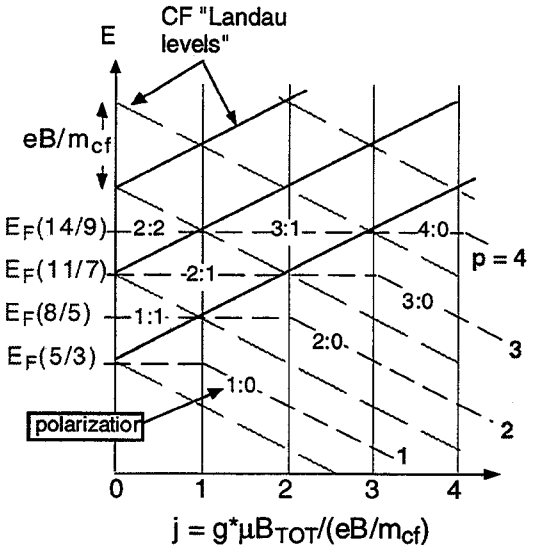

FIG. 4. Schematic of CF Landau level (LL) energies vs. Zeeman energy. When the Zeeman energy is an integer multiple j of the LL energy spacing, the levels cross, producing R_{xx} maxima.

(LLs) is thus $eB_\perp^*/m_{CF}$. However, the model differs from the standard one in that a finite Zeeman energy $g^*\mu B_{TOT}$, determined by the total field, is included. This results in spin-splitting of the CF LLs. By tilting the sample, $g^*\mu B_{TOT}$ can be varied while $eB_\perp^*/m_{CF}$ is held fixed. This situation is illustrated schematically in Fig. 4, where the CF LL energies are plotted vs. Zeeman energy. When $g^*\mu B_{TOT}$ is an integer multiple j of $eB_\perp^*/m_{CF}$, the CF LLs cross. Thus for a fixed electron $\nu=(3p\pm2)/(2p\pm1)$, (where p is the CF LL filling factor) the Fermi level no longer lies in an energy gap, but rather lies within a doubly degenerate CF LL. As a result, R_{xx} at a fixed ν oscillates as θ and hence $g^*\mu B_{TOT}$ is changed, with maxima appearing at integer j. Note that the 5/3 state, corresponding to $p = 1$, does not cross any CF LLs at finite B_{TOT}, and so remains a strong minimum for all θ.

To compare with this model, in Fig. 5 we plot R_{xx} vs. B_{TOT} for constant $\nu=(3p\pm2)/(2p\pm1)$. Maxima are obserrved for all of the states except 5/3, and their anticipated (integer) values of j are indicated. In the upper part of Fig. 6 we summarize this data by plotting the observed positions of the maxima in the B_{TOT} - $B_\perp^*$ plane. In this plane, integer values of j appear as lines emanating from the origin, and are determined by the data points. (A single j=2 line is drawn for the 8/5 and 11/7 states, which give good agreement.) The spin polarizations of each FQHE state as a function of B_{TOT} are indicated by the labeled vertical lines. The lower part of Fig. 6 plots the same data in a different manner. Because $jB_\perp^*/B_{TOT} = g^*m_{CF}/2m_0$, the position of each data point in the B_{TOT} - $B_\perp^*$ plane gives a measure of g^*m_{CF}, which is plotted as a function of $B_\perp^*$. A linear fit to the data yields $g^*m_{CF}/2m_0 = 0.216 \pm 0.016\ (T^{-1})B_\perp^*$.

Our measured value for $g^*m_{CF}/2m_0$ is much higher than that previously obtained[2] for an MBE sample, but our density is also much higher. Since m_{CF} scales as $(B_\perp)^{1/2}$, in

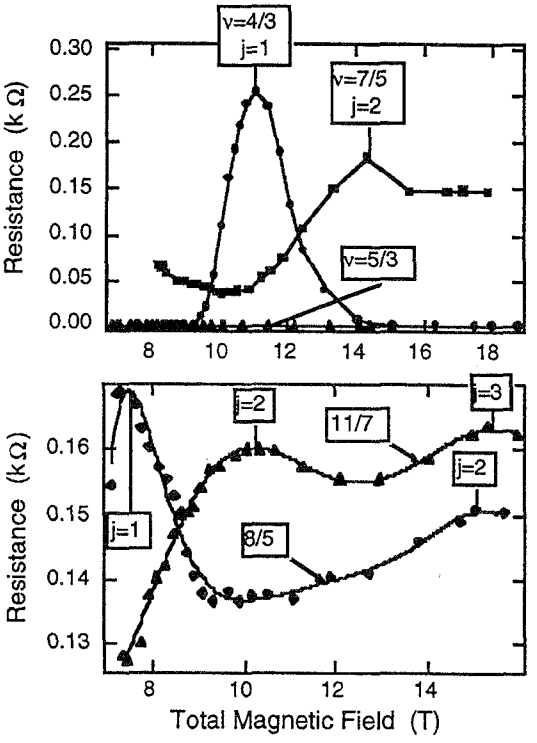

FIG. 5. R_{XX} at fixed ν=(3p±2)/(2p±1) as a function of total field B_{TOT}.

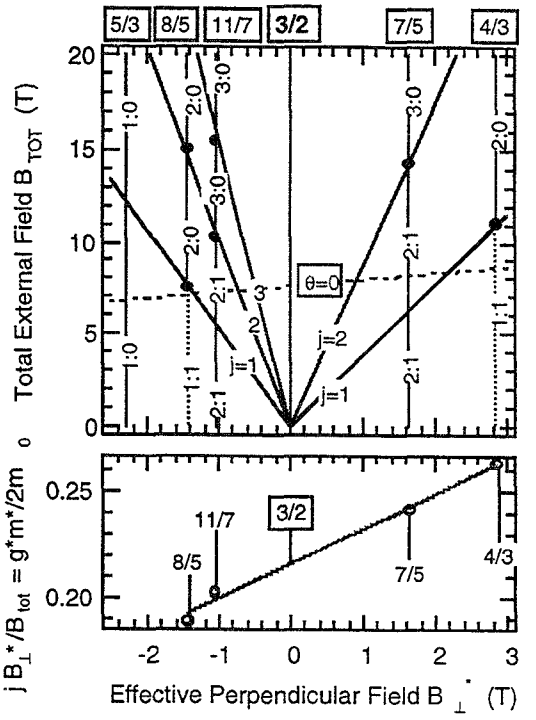

FIG. 6. Upper: Positions of R_{XX} maxima in the B_{TOT}-$B_{\perp}$* plane. Lower: g^*m_{CF} values extracted from the data, and a linear fit. See text.

order to make a comparison the first term in our measured $g^*m_{CF}/2m_0$ must be scaled by $(B_{\perp})^{-1/2}$, while the second term, which contains B*, must be scaled by $(B_{\perp})^{1/2}$. Using a scaling factor of 1.58 we obtain a scaled value of $0.137 + 0.025(T^{-1})B_{\perp}$*, which agrees within experimental error with the value obtained earlier for MBE, $0.132+ 0.023(T^{-1})B_{\perp}$*.

Acknowledgment—This work supported by the U.S. Dept. of Energy under Contract DE-AC04-94AL85000.

References

1. H.C. Chui, B.E. Hammons, N.E. Harff, J.A. Simmons, and M.E. Sherwin, Appl. Phys. Lett. **68**, 208 (1996).
2. R.R. Du, A.S. Yeh, H.L. Stormer, D.C. Tsui, L.N. Pfeiffer, and K.W. West, Phys. Rev. Lett. **75**, 3926 (1995).
3. B.I. Halperin, P.A. Lee, and N. Read, Phys. Rev. B **47**, 7312 (1993).
4. H.C. Chui, B.E. Hammons, J.A. Simmons, N.E. Harff, and M.E. Sherwin, Appl. Phys. Lett. **67**, 1911 (1995).
5. S.P. Watkins and G. Haacke, J. Appl. Phys. **69**, 1625 (1991).
6. T. Makimoto and N. Kobayashi, Jpn. J. Appl. Phys. **32**, 648 (1993); R. Basco, F. Agahi, and K.M. Lau, Appl. Phys. Lett. **63**, 1960 (1993); M. Razeghi et al., Appl. Phys. Lett. **55**, 457 (1989).

Reprinted from:
Proceedings of the Twenty-Fourth State-of-the-Art Program on Compound Semiconductors
Electrochemical Society Proceedings Volume 96-2, p. 186.

ADVANCED FABRICATION TECHNOLOGIES FOR NANO-ELECTRONICS

J.A. Simmons, M.E. Sherwin,* M.V. Weckwerth, N.E. Harff,†
T. M. Eiles,‡ W. E. Baca, H. Hou, and B.E. Hammons
Sandia National Laboratories
Albuquerque, New Mexico 87185-1415 USA

Three novel fabrication technologies are presented which greatly increase the tools available for the realization of nano-electronic devices. First, a sub-micron area post structure descending from a metallic airbridge allows gating of regions as small as 0.1 μm in diameter. This has enabled the study of such quantum phenomena as coupling of parallel quantum point contacts, and electron focusing around a tunable quantum antidot. We also describe two new techniques for backgating multiquantum well structures with submicron lateral resolution. These techniques enable separate ohmic contacts to individual quantum wells spaced as closely as 100 Å, and thus allow the fabrication of novel quantum tunneling devices. The first technique uses regrowth over a patterned ion-implanted substrate. The second involves a novel epoxy-bond-and-stop-etch (EBASE) processing scheme, whereby the original substrate is etched away and the backside then patterned using conventional methods.

SUB-MICRON AIRBRIDGE POST

The use of Schottky gates to modulate submicron areas is of considerable importance in such nanoelectronics research areas as coupled quantum point contacts, [1,2] lateral resonant tunneling through quantum antidot potentials both in the integral [3] and fractional [4-6] quantum Hall effect regimes, and the Aharanov-Bohm effect. [7] The observation of these phenomena requires that the electron phase coherence length, roughly the distance an electron travels before undergoing an inelastic scattering event, be longer than the device dimensions. To obtain these extraordinarily long phase coherence lengths, such structures are typically fabricated in the extremely high mobility two dimensional electron gases (2DEGs) formed in GaAs/AlGaAs heterostructures at low T. While the lateral geometry of nanoelectronic structures in this material can be defined by mesa etching down towards the 2DEG, this technique produces large numbers of electron traps at the etched surfaces and is difficult to control. Rather, it is far more advantageous to form the geometry by using surface Schottky gates to deplete those regions where the electrons are not wanted. [8] This has the additional advantage that the conducting width of the structure can be tuned with gate voltage, since the surface gates also deplete laterally from their edges up to a distance of a few microns. For example, it is this technique that allows the number of one-dimensional subbands in a quantum point contact to be controlled, [9] enabling observation of a conductance quantized in units of $2e^2/h$. However, because this technique

requires that the gate be connected to an external voltage source, those devices which require isolated sub-micron gate-depleted regions, such as the "hole" occurring in the middle of an Aharanov-Bohm ring, present a special challenge.

To meet this challenge, we have developed an integrated metallic air-bridge [10] and submicrometer gate post [2] for use in surface Schottky gates that can be independently biased. The air bridge and gate post are fabricated in a single step and are easily incorporated into existing processes. Previous work on sub-micron gating by Taylor et al. [11] and Simpson et al. [5] focused on the use of an interlevel dielectric to act as a spacer between multiple metal levels. However, the addition of a dielectric spacer adds two processing steps to the fabrication sequence and generally requires dry etching of the dielectric. Further, the plasma processing associated with both dielectric deposition and etching can have a significant deleterious impact on the device. [12] While in this work they used a first level metal disk to protect the semiconductor from plasma damage during the dry etching of the dielectric, since the contact hole must line up with the first level metal disk this method places stringent limitations on the minimum size which can be achieved.

By contrast, the airbridge-and-post process described here requires only one electron beam lithography step followed by a single metal evaporation and lift-off. The final structure leaves the semiconductor surface free of dielectric overlayers and does not involve a potentially damaging dry etch. Here we describe the use of our process to fabricate a pair of parallel quantum point contacts (QPCs) which exhibit coupling to one another. The structure consists of two outer gates of conventional first level metal separated by 1.6 μm, and between them a central gate composed of a 0.2 μm diameter post dropped from an airbridge. As will be shown, when subject to magnetic fields the structure can also be viewed as a quantum antidot potential within a narrow constriction.

The material used was an MBE-grown $Al_{0.3}Ga_{0.7}As/GaAs$ heterostructure with the 2DEG located ~1200 Å beneath the surface. A 250 Å donor layer Si-doped to $1x10^{18}$ cm^{-3} was separated from the 2DEG by a 400 Å $Al_{0.3}Ga_{0.7}As$ spacer layer. The 2DEG has a density of $2.0x10^{11}$ cm^{-2} with a mobility of 10^6 cm^2/Vs, without illumination. Hall bars defined with optical lithography were fabricated by wet etching. Large area Au/Ge/Ni contacts and Cr/Au gate leads were optically defined and deposited by lift-off. The two outer first level gates of the device are then patterned by e-beam lithography and a Cr/Au liftoff.

TABLE 1. Exposures for airbridge/post definition.

Exposure Region	Dose ($\mu C/cm^2$)
2 μm wide lines on GaAs	320
2 μm wide bridges over GaAs	160
2 μm wide bridges over Au	140
Transition dose (line bridge)	250
0.2 μm square gate post	400*

*Results in 0.25 μm diameter post on GaAs.

After the first level gate metallization is complete, the airbridge formation is begun by spinning a bilayer resist profile of 600 nm of PMMA (496K) followed by 1200 nm of P(MMA-MAA) 9%. The P(MMA-MAA) layer is spun on in two coatings of equal thickness.

After each spin the sample is baked on a hot plate at 180°C for 15 minutes. The e-beam exposure of the airbridge structure requires a number of different doses for the different regions of the device, as listed in Table I. A high dose exposes both resist layers to define the large area support pillars and lines. Lower doses expose only the P(MMA-MAA) layer to define the actual bridge region, though because of differing electron backscatter rates this dose depends on whether the bridge crosses a GaAs surface or first level metal. A third, higher dose is used to define the sub-micron gate post. We also make use of a transition dose between the bridging region and the large support pillars. The e-beam lithography system was operated at 50 keV with a beam current of 2 nA. The airbridge is 2.0 μm wide and the contact hole is drawn as a 0.2 μm square hole in the center of the airbridge. After exposure, the sample is developed in MIBK:IPA (1:2) at room temperature for 3 minutes with light agitation. Figure 1 shows an example of the developed resist profile for a similar airbridge structure, clearly demonstrating the ability to selectively open holes to the substrate while maintaining a bridge above the bottom layer of resist. The P(MMA-MAA) layer shows excellent undercut, which allows a clean liftoff profile. Although it is possible to use a tri-level resist profile we have found that the bilayer resist is usually more than adequate for good liftoff. The bottom PMMA layer acts to guide the metal bridge over various topography, including etched facets and first level metal. We have found that the airbridge can span topography that is as tall as the bottom PMMA layer thickness.

Following the resist development, the sample is descummed and dipped in Buffered Oxide Etch (BOE) before loading into the evaporator. For this resist profile a Ti/Au (50/650 nm) metallization is defined by liftoff in acetone. We have previously reported on the fabrication of taller bridging structures with larger dimensions. [2] The process has a good amount of latitude and can be engineered for different applications. In the present application the airbridge is ~0.5 μm above the semiconductor surface and the gate post has

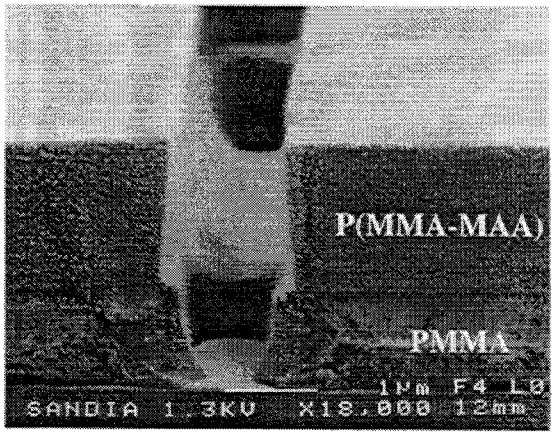

FIG. 1. Resist profile of the bi-layer resist after electron beam exposure and development in MIBK:IPA (1:2). The actual resist thicknesses shown are larger than those quoted in the text.

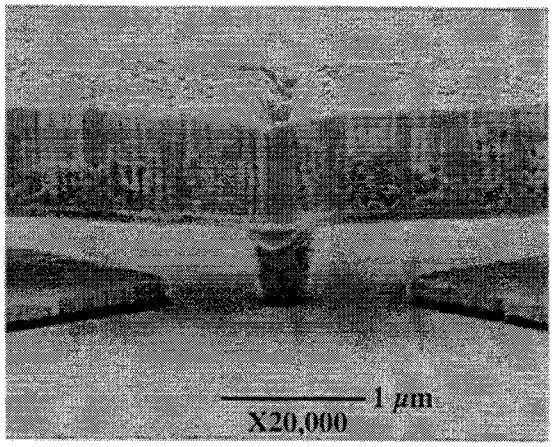

FIG. 2. Completed parallel quantum point contact structure. Side gates are first level metal and the center gate post and airbridge are second level metal. Exposure conditions are listed in Table 1.

a controllable minimum of ≥ 0.1 μm. If the airbridge is lowered so that it is closer to the substrate then it should be possible to fabricate gate posts with even smaller diameters. Figure 2 shows the completed structure with first level gates and the airbridge. Varying the dose from 380 to 440 $\mu C/cm^2$ increases the gate post diameter from 0.1 μm to 0.45 μm.

A similar airbridge approach, albeit for larger critical dimensions, has been previously reported [13] but this technique relies on the use of a complex development sequence for each layer of a tri-layer resist profile. Other techniques have required multiple e-beam exposures and metal evaporations. [14] Our technique uses a single exposure, a single development followed by a single metal evaporation and liftoff, with the advantage that the minimum feature size is not limited by alignment considerations.

The conductance through the parallel QPCs formed on either side of the gate post was measured at 0.1 K using standard low-frequency lock-in techniques. Depletion under the gates occurred at -0.25 V. The gap between either side gate and the center gate post is approximately 0.7 μm. Figure 3 shows the quantized conductance steps for two conditions: (a) all three gates swept together, and (b) with one QPC fully pinched off by a side and center voltage of -5.5 V

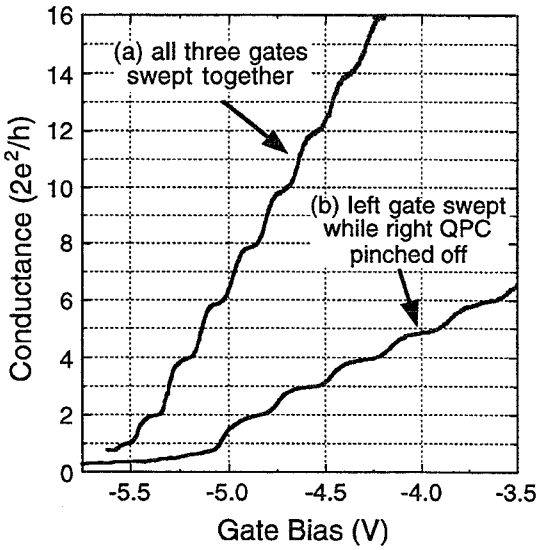

FIG. 3. Quantized conductance steps for the structure in Fig. 2. (a) All three gates swept together, yielding conductance steps of 4 e^2/h and exhibiting quantum coherence between the two QPCs. (b) Same structure with the right QPC fully pinched off and the left gate swept. The conductance steps are in units of 2 e^2/h.

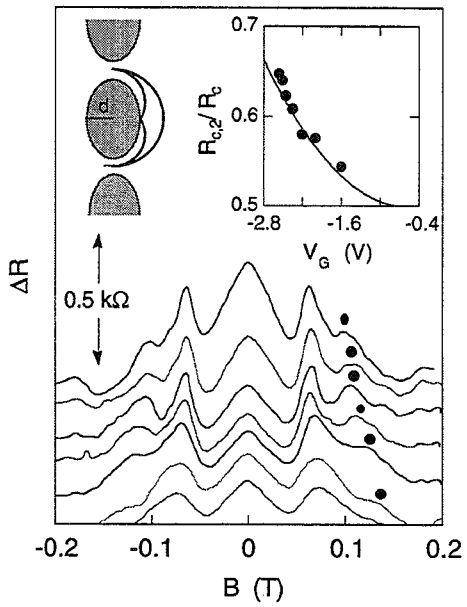

FIG. 4. Magnetoresistance of parallel QPCs with balanced electrical widths, at 0.3 K. Sidegate voltages were fixed at -0.7 V and -0.9 V, while center gate voltages were -1.6, -2.0, -2.2, -2.35, -2.45, -2.50, and -2.55 V. The primary focusing resistance peaks appear near ~0.07 Tesla and their positions change little with center gate bias. However, the positions of the secondary reflection focusing peaks (marked by dots) do change with center gate bias. Left inset: cyclotron orbits for primary and secondary peaks. Right inset: ratio of secondary to primary peak positions, discussed in Ref. 17.

and the other side gate swept. [When the opposite gate is measured in a similar manner, the data is virtually identical to (b).] No gate leakage was measured at any time during the measurements. With one QPC fully depleted, shown in (b), the conductance steps of the device were quantized in units of $2e^2/h$, obviously due to the other QPC. However, when both quantum point contacts were open, shown in (a), the conductance steps were quantized in units of $4e^2/h$. Steps of $4e^2/h$ were observed when all three gates were swept together, or when the center gate was swept with the side gates held at a constant bias. The locking of both QPCs together to produce conductance steps of $4e^2/h$ has been explained with a minimum energy argument by Smith et al. [1] When the two QPCs are within the electron phase coherence length, the QPCs form a coupled system and the sub-bands de-populate together. We note that the two QPCs pinched off at different biases (-5.5 and -5.0 V) when operated independently. SEM inspection of similar devices have shown excellent alignment of the center gate post in the middle of the two side gates, so we are forced to attribute this difference to random potential fluctuations in the channels.

The two QPCs in parallel can also be viewed as a narrow constriction with an antidot potential in the center. Thus the sample also exhibits electron focusing phenomena when a magnetic field B is applied. Earlier observations of magnetic focusing either used separated QPCs which could not be measured in parallel, [15] or occurred in large arrays of quantum dots in which the individual electron orbits were ensemble averaged [16] The structure in Fig. 2 allowed the first observation of focusing around a single antidot. [17]

Magnetic focusing in our structure occurs when the magnetic field B has a value such that an electron passing ballistically through one QPC is bent by B along a cyclotron orbit and focused back into the opposite QPC. As a result, the electron is localized around the antidot, and the resistance of the device increases. In Fig. 4 we show the $T = 0.3$ K magnetoresistance of the sample when the electrical widths of the two QPCs have been carefully balanced, and the bias on the central gate is stepped so as to vary the size of the antidot potential. A primary magnetic focusing peak is present at a nearly constant B of ~±0.07 T, in agreement with a simple calculation based on the geometry of the device. [17] Also discernible is a secondary focusing peak, arising when the electron has a narrower cyclotron orbit and is specularly reflected in a single bounce off the antidot potential. (See sketch inset in Fig. 4.) The position of the secondary reflectance peak depends on the

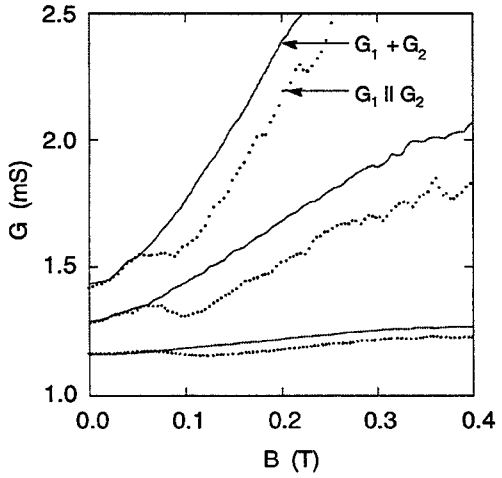

FIG. 5. Low field magnetoconductance at three bias conditions of the two QPCs measured in parallel (dots), and the *sum* of the conductances of the two QPCs measured individually (solid line). Ohm's law is clearly violated.

size of the antidot and hence the bias of the central gate, while the position of the primary peak depends only on the QPC positions, which are relatively unchanged. The right inset plots the ratio of the cyclotron radii for the primary and secondary peaks as a function of gate voltage, along with a fit based on this model. [17]

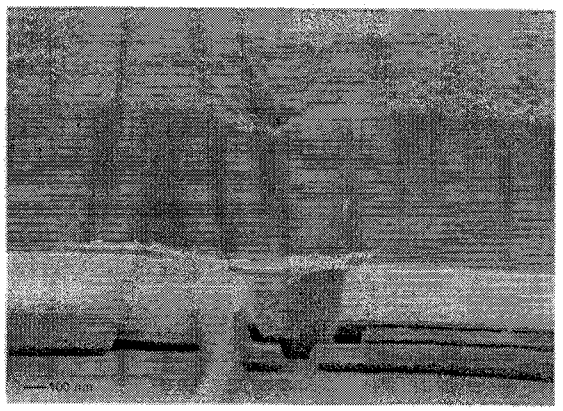

FIG. 6. Photo of Coulomb blockade device with a post/airbridge gate positioned over the quantum dot region. Biased positively, the post gate should deepen the dot potential and allow observation of the Coulomb blockade at higher temperatures.

We note that magnetic focusing in these structures produces a violation of Ohm's law: the conductance of the two QPCs measured in parallel *is not equal* to the sum of the conductances measured individually. In Fig. 5 is the magneto-conductance (MC) of an identical geometry structure fabricated in lower electron density material, for three bias conditions. [17] While the sum of the individual QPC MCs (lines) is fairly monotonic, the parallel MC (dots) displays the conductance dip corresponding to the focused orbit, and then follows the shape of the single QPC sum, though there is a constant conductance deficit that persists to higher B.

Although to date we have only performed electrical measurements on the coupled parallel QPC type of structure, we believe that the airbridge/gate post process will have great utility in future research on additional types of nanoelectronic structures. In Fig. 6 is shown a Coulomb blockade structure in which a submicron post-gate is positioned over the quantum-dot or island region of the device. Such a gate should allow the depth of the dot's confinement potential to be maintained with a positive post-gate voltage, while the dot is made narrower by negative side gate voltages. This should allow the energy level spacings to be made much larger, thus increasing the temperature at which the device can operate.

BACKGATING OF MULTIQUANTUM WELL STRUCTURES

The strong current interest in the behavior of double quantum well (DQW) structures was largely precipitated by two pioneering works. Boebinger et al. [18] demonstrated that at high magnetic field B such double 2DEG systems can form a correlated bilayer state, in which the positions of electrons in one QW are correlated with those in the other so as to minimize the total energy of the system. Palevski et al. [19] demonstrated that the coupling between a high mobility QW and a closely spaced low mobility QW could be controlled, yielding a switchable mobility edge and promising future device possibilities. While these experiments only used contacts to the two QWs in parallel, it was soon realized that the ability to make electrical contact to the individual QWs, even though they are spaced apart by a barrier whose width is only on the order of 100 Å, would enable a number of experiments which could much more effectively probe

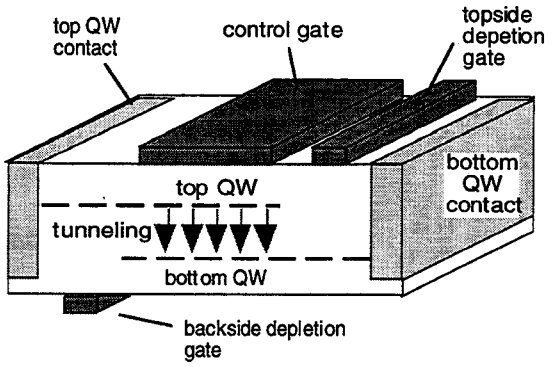

FIG. 7. Sketch of the selective gate depletion method of making independent contacts to DQW structures. Geometry shown is for an interwell tunneling configuration.

both tunneling and Coulomb interactions between electrons in adjacent QWs. Ground breaking work in making independent contacts was performed by Eisentein et al., [20] who developed a selective backgating technique. In the backgating scheme, each contact is comprised of two parts: a diffused metallic contact which reaches both of the QWs, and a gate which locally depletes electrons from the QW which one does *not* wish to contact. (See Fig. 7.) Whereas a contact to the bottom QW uses a gate on the top surface, a contact to the top QW requires a backgate. (It is of course easy to extend this scheme to structures with more than two QWs by simply using both a top gate and a backgate for each contact.) This technique allowed numerous other pioneering experiments on electron-electron interactions, including measurements of 2D-2D inter-QW tunneling as a function of gate bias, [21] in-plane magnetic fields, [22] and perpendicular magnetic fields, [23] and a measurement of Coulomb drag, [24] in which the "frictional" drag of a current flowing in one QW causes a voltage to be developed in the other QW.

In the implementation of Eisenstein et al., the backgates were simply patterned by conventional metallization and lift-off on the back surface of the substrate, after mechanically lapping it to a thickness of ~50 μm. This has the significant disadvantages of poor lateral resolution (on the order of the substrate thickness), and requires high operating biases (approaching 100 V) in order to fully deplete one of the quantum wells. Further, handling of samples of such minimal thickness requires extreme care. More recently, backgates have been fabricated by using a focused ion-beam to damage a conducting layer in the substrate before growth of the active layers. [25] While submicron structures are possible, this technique requires expensive focused ion-beam equipment, available in only a few laboratories. The same group has also fabricated backgate structures by using a shallow-angle etch to form the backgate pattern in a bulk doped layer, and then regrowing active layers upon the etched surface. [26] This last technique requires regrowth on a non-planar structure, is limited in spatial resolution by the edges of the shallow angle etch, and is complicated by the fact that the material regrown on the relatively large etched facets is likely to have different doping efficiency, electron density, and mobility.

Described here are two novel techniques we have developed for submicron backgating of MQW structures. In the first, backgates are ion-implanted through a SiN mask into a virgin undoped GaAs substrate. The active MQW layers are then regrown over the planar implanted substrate. In the second technique, a novel wafer epoxy-bond-and-stop-etch (EBASE) method is used. After processing of the front side, the wafer is epoxy-

bonded front-side down onto a new GaAs host substrate. The original substrate is then removed by mechanical lapping followed by a wet chemical etch down to a stop etch layer incorporated into the grown buffer. Backgates are then added to the exposed backside of the epitaxial layers, using conventional metallization and lift-off.

Laterally Patterned Ion-Implanted Backgates

In the ion-implanted backgate technique, the first step is to deposit 1 μm of SiN on clean epi-ready 3" GaAs substrates. Because the ion-implanted pattern will not be visible, it is necessary to place alignment marks in the substrate. This is done by patterning the SiN with photoresist, etching through the SiN with a Buffered Oxide Etch (BOE), and then using 1:1:8 H_3PO_4:H_2O_2:H_2O to etch the alignment marks ~6000 Å into the GaAs. The wafer is than again coated with photoresist, which is exposed and developed with the backgate pattern. The SiN is again etched with BOE, opening windows in the SiN mask for the implant. The photoresist is then stripped in acetone, and the wafer is cleaned in an O_2 RF plasma at 850 mTorr for 30 minutes at 75 W. The resulting SiN-masked wafer is then given the following three ^{29}Si implants at a 7° tilt: 2×10^{13} cm^{-2} at 40 keV, 2×10^{13} cm^{-2} at 100 keV, and 8×10^{13} cm^{-2} at 200 keV. Secondary ion mass spectroscopy (SIMS) data shows that the implants result in a layer ~0.25 μm thick containing ~4×10^{18} cm^{-3} Si. The SiN is then removed using BOE. We note that, except for the relatively tiny alignment marks, at no point during the implant process do any organics come into contact with the substrate.

Because initial test wafers fabricated using this technique exhibited implanted backgates that had a tendency to leak to one another, two *p*-type blanket implants are performed at this point. The dose is kept sufficiently low that the Si-implant is only slightly compensated, yet high enough that *p-n* junctions are formed, both beneath and at the edges of the backgates, for isolation. The implants used are both Be at 7° tilt: 7.5×10^{11} cm^{-2} at 40 keV, and 2.0×10^{12} cm^{-2} at 200 keV. This results in a layer ~0.8 μm thick containing ~3×10^{16} cm^{-3} Be.

The wafer is then given a rapid thermal anneal at 850 °C for 20 seconds to activate the implant, and is at this point ready to have the active layers regrown on it. Because of its superior regrowth capabilities, we use a metalorganic chemical vapor deposition (MOCVD) reactor which has recently shown record mobilities. [27] A typical layer structure contains two QWs separated by a ~100 Å barrier, and is as follows: 1500 Å GaAs buffer, an 8 period superlattice of 150 Å $Al_{0.45}Ga_{0.55}As$/ 600 Å GaAs, 1000 Å $Al_{0.3}Ga_{0.7}As$, 200 Å $Al_{0.3}Ga_{0.7}As$ doped 2×10^{18} cm^{-3}, a 500 Å $Al_{0.3}Ga_{0.7}As$ spacer layer, 150 Å wide GaAs bottom QW, a 100 Å $Al_{0.3}Ga_{0.7}As$ barrier, 150 Å wide GaAs top QW, a 500 Å $Al_{0.3}Ga_{0.7}As$ spacer layer, 200 Å $Al_{0.3}Ga_{0.7}As$ doped 2×10^{18} cm^{-3}, 500 Å $Al_{0.3}Ga_{0.7}As$, and a 30 Å GaAs cap layer. The high Al content in the superlattice buffer is found to be effective in preventing leakage between the backgates and the active QWs.

After regrowth, the wafer is cleaved into individual samples, which are then patterned into Hall bars using a conventional mesa etch, and aligning to the marks

previously etched into the substrate. Vias are then etched down to the implanted backgates, and Au/Ge/Ni contacts are evaporated both in the vias and on the arms of the Hall bar. The ohmic contacts are annealed at 420 °C for 90 seconds, and then top gates are deposited using standard metallization and lift-off.

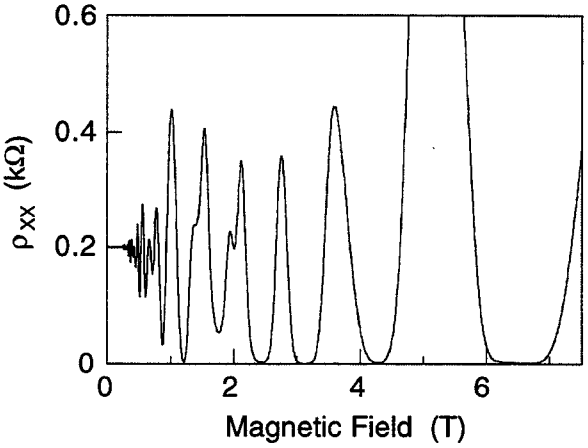

FIG. 8. Magnetoresistance of the DQW regrown by MOCVD over the implanted back gates. All gates were grounded. High quality of the quantum Hall effect states is apparent.

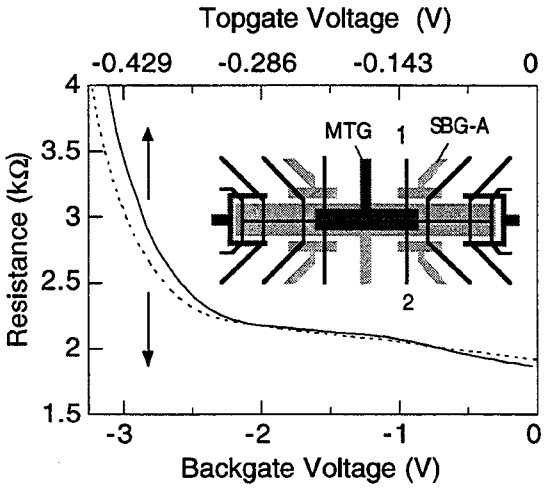

FIG. 9. Two-terminal resistance (contacts 1 & 2) as a function of gate bias for the main topgate (solid line), and a side backgate (dotted line). The two voltage scales differ by a factor of 7, the ratio of the gates' distance to the DQW layers. Inset: mesa (black lines), backgates (light gray), and topgates (dark gray).

The resulting back gated DQW samples are of excellent quality, with the implanted regions completely invisible under a microscope. The samples were measured at 0.3 K using standard low frequency lock-in techniques. With all gates unbiased, the sample whose growth structure is given above exhibited a total density of 3.2 x 10^{11} cm^{-2} and mobility of ~1.0 x 10^5 cm^2/Vs. In Fig. 8 we show the magnetoresistance of the sample to 7.5 Tesla, with all gates grounded. The high quality of the quantum Hall effect states is a good indication of the excellent quality of the MOCVD regrowth, and shows the dual period oscillations characteristic of DQWs. For this particular sample, a main backgate lay under the entire length of the Hall bar, and so four-terminal measurements of regions *not* over the backgate could not be performed. (See Fig. 9 inset.) However, for previously measured samples without the *p*-type implant the main backgate lay under only half the Hall bar. In those samples the density and mobility of regions regrown over the backgate were found to be identical to those regrown elsewhere, and of similarly good quality to the present sample.

In Fig. 9 we show the resistance between leads 1 and 2 (see inset) as a function of bias on

side backgate SBG-A, and also as a function of bias on the main topgate MTG, in each case with all other gates grounded. A plateau is seen at ~-2.2 V for the backgate, corresponding to the depletion of the bottom QW only. A similar plateau appears at a bias of -0.3 V on the topgate, corresponding to depletion of the top QW only. At a bias of -4 V for the backgate, and -0.6 V for the topgate, both QWs are depleted, causing the resistance to diverge. The other backgates exhibited almost identical behavior. We note that the shapes of the two curves are extremely similar, except for a factor of ~7 in gate voltage. (To emphasize this similarity the figure has both top and bottom axes, whose scales differ by a factor of 7.) This is almost identical to the 7.1 ratio of the distances of the top and backgates from the DQW electron layers, as expected.

The Epoxy-Bond-And-Stop-Etch (EBASE) Technique

We have also developed a different method for backgating MQW structures, which requires neither ion-implantation nor regrowth. This epoxy-bond-and-stop-etch (EBASE) technique enables the definition of mesas, Schottky gates, and ohmic contacts on the backside as well as the front, since the backside surface is made only a few 1000 Å away from the active layers. Essentially, the technique consists of processing the front side of the wafer, defining any mesas, ohmic contacts, and Schottky gates that are required. The sample is then epoxied front-side-down onto a host substrate to provide physical support. The original sacrificial substrate is then removed by mechanical lapping, followed by chemical etching to a stop-etch layer which has been incorporated into the grown buffer. The resulting exposed backside surface is on the order of 1 μm away from the active layers, and is free to be processed by conventional methods. Electrical contacts to the patterned front side are provided by etching via holes through to the front side ohmic metal and Schottky gates. The finished structure is robust against repeated cycling to liquid He temperatures, exhibiting no signs of cracking, stress, or flaking. The low T transport characteristics of samples fabricated in this manner are identical to those that have not undergone the wafer-bond-and-etch process, demonstrating that the process has no deleterious effects on sample quality.

Previous work done on flip-chip processing techniques has focused on either eutectic metal bonding, where the two surfaces become bonded by a heated metal layer diffusing simultaneously into the two substrates, [28] or by van der Waals forces created between the highly polished substrate surfaces. [29] The latter technique requires extensive and sophisticated processing in order to achieve the exceptionally clean and smooth surfaces needed, while the thermal annealing required in the former may damage such delicate structures as electron-beam defined gates. Further, it is not clear whether these techniques can be used on the highly non-planar surfaces presented by conventional mesas, contacts, and gate structures. By contrast, our EBASE technique can be used on surfaces with features up to a few microns in height, and requires no special cleaning procedures. We note that while recently Bhattacharya et al. [30] have used a similar technique in the fabrication of FETs, they did not report on the lateral extents of the bonded regions and whether the structures were tested at liquid He temperatures. To our knowledge, the

present paper reports the first use of this method in the selective gating of MQW structures.

The starting point in the fabrication sequence is the incorporation of the stop etch layer into the buffer of the MQW structure, grown either by MBE or MOCVD. We have found that the design of the buffer is important and must address two potential concerns. First, it must be possible to obtain a high selectivity of etch rates between the sacrificial GaAs substrate and the stop-etch layer. We use a citric acid selective etch buffered with H_2O_2 in the ratio 6.5:1 (citric:H_2O_2), which etches GaAs much faster than $Al_xGa_{1-x}As$. [31] While this etch solution in general shows a greater selectivity for higher Al content, we have found that a pure AlAs stop etch layer leaves a very rough surface after etching, presumably due to oxidation of the finished surface. On the other hand, $Al_{0.3}Ga_{0.7}As$ exhibits a selectivity over GaAs of only ~100, [31] which is somewhat low for our purposes. We have found that the higher aluminum content of a layer of $Al_{0.72}Ga_{0.28}As$ constitutes a reasonable compromise, exhibiting selectivities so high that they are difficult to measure, yet yielding an extremely smooth surface for patterning. The second concern is that the backside Schottky gates not leak through the buffer into the active layer. While the high Al content of the stop etch layer helps to prevent leakage, the growth of an $Al_xGa_{1-x}As$/ GaAs superlattice is found to further reduce the leakage current.

In this paper we focus on results from a high-quality DQW wafer grown by MOCVD. Details of the growth conditions have been given elsewhere. [32] A 1000 Å GaAs buffer layer is first grown, followed by a 1 μm thick $Al_{0.72}Ga_{0.28}As$ stop etch layer. Another 5000 Å of GaAs is then grown, followed by a 10-period superlattice of 100 Å $Al_{0.3}Ga_{0.7}As$ / 30 Å GaAs. At this point a standard DQW structure is grown, consisting of 2000 Å of $Al_{0.3}Ga_{0.7}As$, 200 Å of $Al_{0.3}Ga_{0.7}As$ doped n-type at 1×10^{18} cm^{-3}, a 500 Å $Al_{0.3}Ga_{0.7}As$ bottom spacer layer, the 150 Å GaAs bottom QW, a 100 Å $Al_{0.3}Ga_{0.7}As$ tunnel barrier, the 150 Å GaAs top QW, a 500 Å $Al_{0.3}Ga_{0.7}As$ top spacer layer, 200 Å of $Al_{0.3}Ga_{0.7}As$ doped n-type at 1×10^{18} cm^{-3}, and another 500 Å of $Al_{0.3}Ga_{0.7}As$. Finally, a 30 Å cap layer of GaAs doped n-type at 1×10^{18} cm^{-3} is grown.

The front side of the structure is then patterned using conventional methods. A Hall bar pattern is mesa-etched to a depth of 1500 Å, and Au/Ge/Ni contacts are evaporated on the ends of the Hall bar and annealed 90 seconds at 420 °C. Several front-side Schottky gates composed of 200 Å Ti / 2000 Å Au are then deposited by evaporation and lift-off.

After the front side processing is complete, the sample is ready to be epoxied to the host support substrate. It is important to use a host substrate whose lateral extent is smaller than that of the sacrificial substrate, so that the edge bead of epoxy which is squeezed out from the two substrates does not interfere with subsequent backside lithographic processing steps. Gatan Inc. Type G-1 epoxy, a low viscosity heat-cured epoxy commonly used for the preparation of transmission electron microscopy samples, is used to bond the samples. The epoxy and hardener is mixed following the manufacturers instructions, and is allowed to sit for 10 minutes so that any air bubbles present will dissipate. A dab of epoxy is then placed on the front side of the active wafer, and the host substrate is placed smooth-side down on the epoxy. Gentle downward pressure is applied

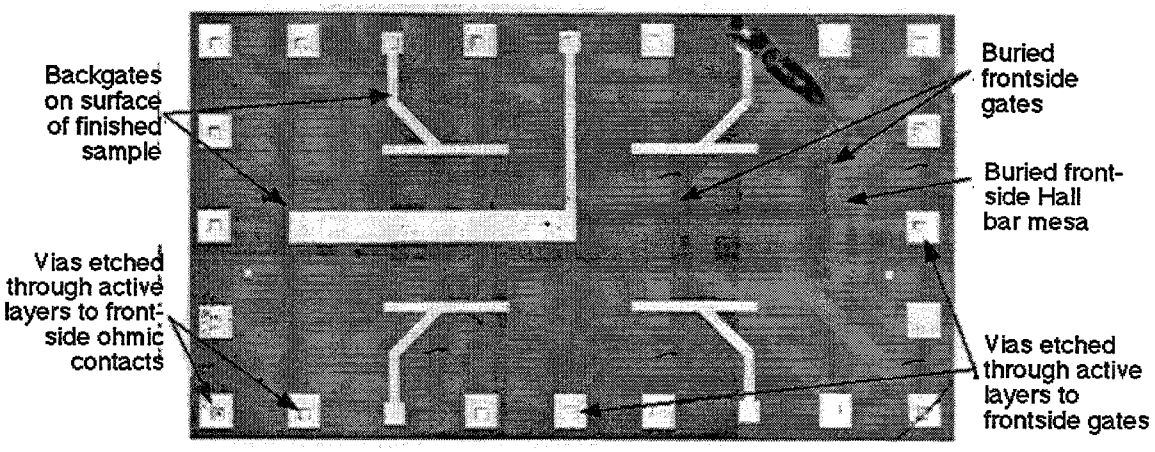

FIG. 10. Image of a completed 2 μm thick EBASE structure that has been patterned on both sides. The brightest regions are the backgates and metal pads over the via holes, both located on the now-exposed back surface. Also visible are the Hall bar mesa and front side gates, now buried under the 2 μm thick active layers. The image is a montage of several photos taken with infrared illumination.

to the host substrate while it is slid back and forth, forcing the layer of epoxy to become relatively thin, on the order of 2 μm. The sample is then baked on a 100 °C hotplate for ~30 minutes to cure the epoxy.

Once the epoxy has hardened, the original sacrificial substrate on which the active layers were grown is removed. Because of the relatively slow etch rate and poor uniformity of the selective citric acid etch, most of the substrate is first removed by mechanical lapping using a 3 μm Al_2O_3 grit, with the sample attached by wax to a glass puck. When only ~25 μm of the sacrificial substrate remains, the sample is removed from the lapping apparatus and cleaned. After attaching the host substrate side of the sample to a glass cover slip using wax, the sample is then placed in the citric acid selective etch to remove the remaining GaAs sacrificial substrate, which takes on the order of 1-2 hours. Because the etch is non-uniform, the surface appears very rough until the $Al_{0.72}Ga_{0.28}As$ stop etch layer is exposed, at which point it acquires a mirror finish.

At this point via holes are etched through the active layers to the (now buried) front side electrical contact pads for the gates and ohmics. On the same evaporation step, 200 Å Ti/ 2000 Å Au is deposited in the via holes, and also in the backside Schottky gate pattern. One mil Au wires are then attached to the contact pads using 50/50 In/Sn solder applied with a soldering iron at 200 °C. The sample is quite robust against the elevated temperatures of photoresist baking at 90 °C and the solder temperatures of 200 °C, with no deleterious effects observed. The effects of higher temperatures will be discussed below.

In Fig. 10 we show an image of the completed sample, before the Au lead wires have been attached. The sample was imaged with infrared, making the buried frontside patterns visible through the 2 μm thick active layers. The lightest regions are the backside gates and via metallization pads, residing on the exposed surface of the sample. The buried

Hall bar mesa pattern and frontside Schottky gates appear as light gray regions. While a lithography-related defect is visible in the upper right corner of the sample, we note that no cracking or peeling is present anywhere else. After repeated temperature cyclings to 0.3 K, the appearance of the structure and its low temperature electrical characteristics remained unchanged. The total lateral extent of the sample is ~ 8 mm x 4 mm, giving the single crystal active layer an aspect ratio of ~4000:1. Fig. 11 is a scanning electron micrograph of the edge of a similar sample after cleaving. Because the crystal planes of the active layers are not perfectly aligned with those of the host substrate, the cleaved edge of the active layers is rather rough. Nonetheless, the smooth surface of the stop etch layer is readily apparent, and the epoxy thickness is ~2 μm.

The sample's electrical characteristics were measured at 0.3 K in a top-loading pumped ^{3}He system using standard low frequency lock-in techniques. Fig. 12 shows the four terminal resistivity of a region over the main central backgate, as a function of backgate bias, with all other gates unbiased. The resistance increases as the bottom QW is depleted. At ~-3.4 V, the bottom QW is entirely depleted and a plateau is formed. At higher gate biases the top QW also begins to deplete, becoming completely depleted at ~ -7 V. In Fig. 13 we show the longitudinal resistivity as a function of B for several different backgate biases: (a) 0.0 V, (b) -1.0 V, (c) -2.0 V, and (d) -3.5 V. In (a) the 2D electron densities of the two QWs are equal to one another, at ~2.1 x 10^{11} cm^{-2} for each QW. (Each QW also has the same mobility, ~3.3 x 10^5 cm^2/Vs.) As a result, the Shubnikov-de Haas (SdH) oscillations from each well are identical, and so reinforce one another and do not exhibit beating. In (b) the densities of the two QWs are different, the top QW having been partially depleted, and a beating of the SdH oscillations at low B is readily apparent. In (c) the density difference has become even greater, causing the beating to become more rapid, and the minimum at Landau level filling factor ν=2 near 8 Tesla to no longer reach zero. Finally, in (d) the bottom QW has been fully depleted, and only a single period of SdH oscillations from the top QW is apparent. Because the density in the top QW is still nearly 2.1 x 10^{11} cm^{-2}, the period of the SdH oscillations is nearly the

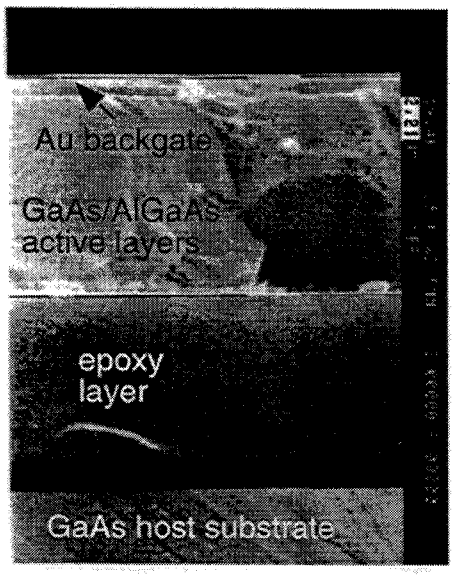

FIG. 11. SEM of the edge of an EBASE sample.

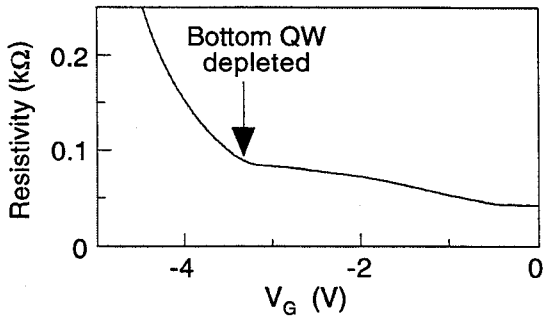

FIG. 12. Four terminal resistance vs. backgate voltage for an EBASE sample. A clear plateau appears when the bottom QW becomes depleted.

same as in (a), only the oscillations are now due to the top QW only.

By performing Fourier transforms in $1/B$, the electron densities in each QW can be determined. In Fig. 14 we summarize the densities as a function of backgate bias. The total density depends nearly linearly on backgate voltage, while the top QW density remains relatively unchanged as long as some electrons remain in the bottom QW. We note that the effect of the backgate on the DQW is virtually identical to that of the top gate, except that

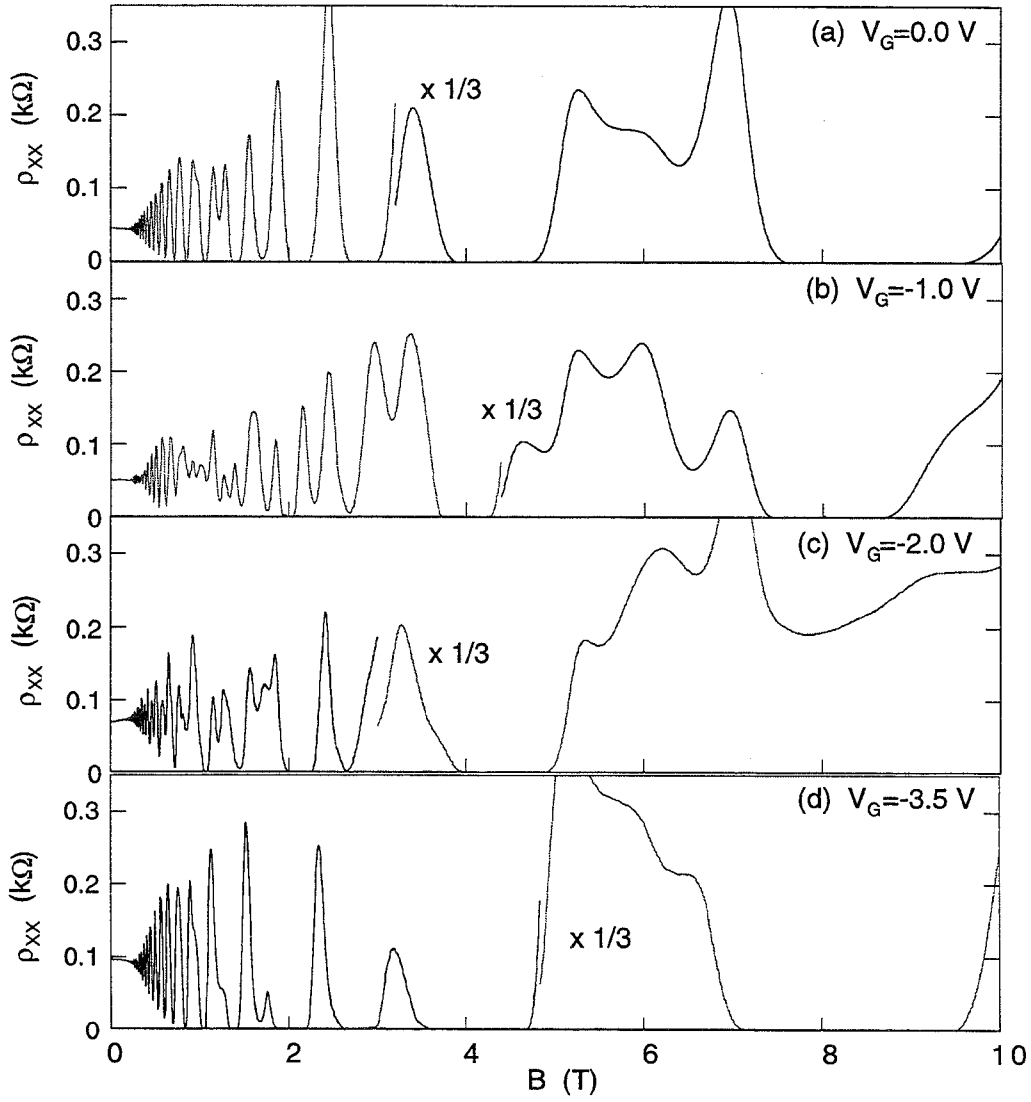

FIG. 13. Four terminal longitudinal resistivity as a function of B for four different backgate voltages. In (a) the two QWs have identical densities, producing "clean" quantum Hall effect oscillations without beating. In (b) and (c) the densities are imbalanced, producing substantial beating. In (d) the bottom QW is entirely depleted, and the oscillations, similar in appearance to (a), are from the top QW only.

the voltage scale is approximately a factor of 12 larger. This is in rough agreement with the factor of 14.6 greater distance of the backgate from the DQW layers.

We have tested the EBASE technique with active layers as thin as 2000 Å, also at lateral extents of 8 mm. Because, when defined by depletion, the lateral resolution of electrically conducting regions is limited to the distance between the gates and the active layers, this technique should allow submicron geometries to be defined by backgating, simultaneously with front-gating. Since the samples are clearly able to withstand temperatures of 200 °C, PMMA bake temperatures will not present a problem and electron-beam defined structures can be patterned on the backside. This should enable the construction of novel mesoscopic devices in MQW structures, such as Aharanov-Bohm interferometers in which the interference paths are the two QWs, [33] or novel quantum tunneling transistors. [34,35]

We have also attempted other processing steps on the EBASE sample backsides, including mesa etching and ohmic contact formation. On a sample which had no frontside processing, a Hall bar was mesa etched from the backside down to the epoxy, leaving it "freestanding", and Au/Ge/Ni contacts were evaporated over the ends of the Hall bar. At this point the Hall bar definition appeared excellent, with no cracking or peelin. The sample was then annealed at 400 °C for 60 seconds to drive the ohmic metallization into the electron layers. Some outgassing from the epoxy was observed during this process. After annealing, bands of discolored regions appeared throughout the 200 μm wide Hall bars. We believe that these are due to the active layer becoming locally unbonded from the epoxy. The sample was then measured at 0.3 K, and despite the local unbonding, was seen to have excellent electrical characteristics, nearly identical to Hall bars manufactured from the same wafer without the EBASE technique. We expect that with further work it should be possible to develop a process for making ohmic contacts without causing such unbonding, either by using ohmic contact metallizations such as Pd/Ge which do not require such high temperature anneals, or by using other epoxies.

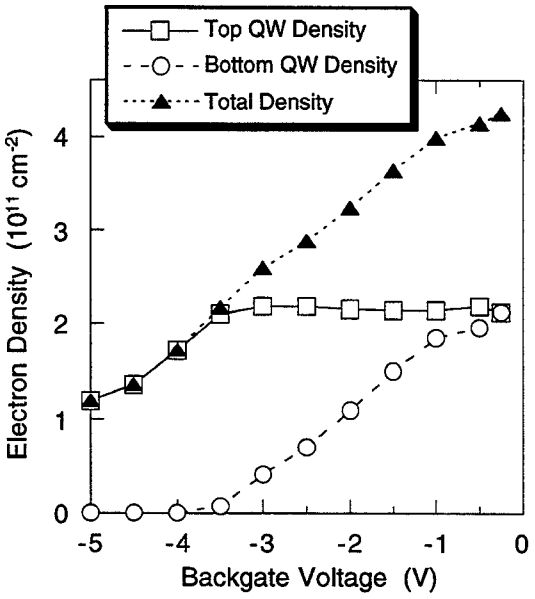

FIG. 14. Top QW density, bottom QW density, and total density in the EBASE sample as a function of backgate voltage. The top QW density remains constant as long as electrons remain in the bottom QW, while the total density is nearly linear with backgate bias.

In summary, we have presented three novel fabrication technologies for nano-electronic structures. First, we described a process for the fabrication of ≥ 0.1 μm diameter Schottky gate posts with integrated airbridges, for use in the construction of quantum interference devices, and quantum dot and antidot structures. Second, we described a simple and inexpensive method for backgating MQW structures by regrowing over patterned ion-implanted substrates. The method allows the use of low gate bias voltages, and should be amenable to submicron resolution. Finally, we introduced a novel EBASE process in which the patterned front side of a wafer is epoxied to a host substrate, and the original sacrificial substrate removed by etching to a stop-etch layer. The technique exposes a high quality backside surface, as close as a few 1000 Å to the active layers, for further processing by conventional methods including e-beam lithography. The EBASE samples are robust against temperature cycling up to +200 °C and down to 0.3 K. Initial results indicate that with some development the EBASE process will also be amenable to mesa etching and ohmic contact evaporation and annealing.

ACKNOWLEDGMENTS

Work supported by U.S. Dept. of Energy Contract No. DE-AC04-94AL85000.

REFERENCES

*Present address: Microwave Signal Inc., Clarksburg, MD 20871.
†Also at Oregon State University, Corvallis, OR 97331.
‡Present address: Intel Corp., San Jose, CA.

[1] C. G. Smith et al., J. Phys. Condens. Matter **1**, 6765 (1989).
[2] M. E. Sherwin, J. A. Simmons, T. M. Eiles, N. E. Harff, and J. F. Klem, Appl. Phys. Lett. **65**, 2326 (1994).
[3] S. W. Hwang, J. A. Simmons, D. C. Tsui, and M. Shayegan, Phys. Rev. B **44**, 13497 (1991).
[4] J. A. Simmons et al., Phys. Rev. Lett. **63**, 1731 (1989).
[5] P. J. Simpson et al., Surf. Sci. **305**, 453 (1994).
[6] C. J. B. Ford et al., J. Phys. Condens. Matter **6**, L275 (1994).
[7] G. Timp et al., Phys. Rev. Lett. **58**, 2814 (1987).
[8] T. J. Thornton, M. Pepper, H. Ahmed, D. Andrews, and G. J. Davies, Phys. Rev. Lett. **56**, 1198 (1986).
[9] B. J. Van Wees et al., Phys. Rev. Lett. **60**, 848 (1988).
[10] M. E. Sherwin, R. Corless, and J. R. Wendt, J. Vac. Sci. Technol. B **11**, 339 (1993).
[11] R. P. Taylor, J. A. Adams, M. Davies, P.A. Marshall, and R. Barber, J. Vac. Sci. Technol. B **11**, 628 (1993).
[12] A. J. Murrell et al., Proceedings of the GaAs IC Symposium, 1992, p. 173.
[13] A. Ketterson et al., J. Vac. Sci. Technol. B **10**, 2936 (1992).
[14] R. G. Woodham et al., Microelectron. Eng. **17**, 563 (1992).
[15] H. Van Houten et al, Phys. Rev. B **39**, 8556 (1989).

[16] D. Weiss et al., Phys. Rev. Lett. **66**, 2790 (1991).
[17] T. M. Eiles, J. A. Simmons, M. E. Sherwin, and J. F. Klem, Appl. Phys. Lett. **52**, 10756 (1995).
[18] G. S. Boebinger, H. W. Jiang, L. N. Pfeiffer, and K. W. West, Phys. Rev. Lett. **64**, 1793 (1990).
[19] A. Palevski, F. Beltram, F. Capasso, L. N. Pfeiffer, and K. W. West, Phys. Rev. Lett. **65**, 1929 (1990).
[20] J. P. Eisenstein, L. N. Pfeiffer, and K. W. West, Appl. Phys. Lett. **57**, 2324 (1990).
[21] J. P. Eisenstein, T. J. Gramila, L. N. Pfeiffer, and K. W. West, Phys. Rev. B **44**, 6511 (1991).
[22] See Ref. 21. We note that inter-QW tunneling can also be measured using only top gates, though less flexibly. See J. A. Simmons et al., Phys. Rev. B **47**, 15741 (1993).
[23] J. P. Eisenstein, L. N. Pfeiffer, and K. W. West, Phys. Rev. Lett. **68**, 3804 (1992).
[24] T. J. Gramila, J. Eisenstein, A. H. MacDonald, L. N. Pfeiffer, and K. W. West, Phys. Rev. Lett. **66**, 1216 (1991).
[25] E. H. Linfield, G. A. C. Jones, D. A. Ritchie, and J. H. Thompson, Semicond. Sci. Technol. **8**, 415 (1993); and K. M. Brown, E. H. Linfield, G. A. C. Jones, D. A. Ritchie, and J. H. Thompson, J. Vac. Sci. Technol. B **11**, 2493 (1993).
[26] R. J. Evans et al., Appl. Phys. Lett. **65**, 1943 (1994).
[27] H. C. Chui, B. E. Hammons, N. E. Harff, J. A. Simmons, and M. E. Sherwin, Appl. Phys. Lett. **68**, 208 (1996).
[28] R. Venkatasubramanian, M. L. Timmons, T. P. Humphreys, B. M. Keyes, and R. K. Ahrenkiel, Appl. Phys. Lett. **60**, 886 (1992).
[29] E. Yablonovitch, T. Gmitter, J. P. Harbison, and R. Bhat, Appl. Phys. Lett. **51**, 222 (1987).
[30] U. Bhattacharya et al., Elect. Dev. Lett. **16**, 357 (1995).
[31] C. Juang, K. J. Kuhn, and R. B. Darling, J. Vac. Sci. Technol. B **8**, 1122 (1990); and G. C. DeSalvo, W. F. Tseng, and J. Comas, J. Electro. Chem. Soc. **139**, 831 (1992).
[32] H. C. Chui, B. E. Hammons, J. A. Simmons, N. E. Harff, and M. E. Sherwin, Appl. Phys. Lett. **67**, 1911 (1995).
[33] Masahiro Okuda et al., Phys. Rev. B **47**, 4103 (1993).
[34] J. A. Simmons, M. E. Sherwin, N. E. Harff, and J. F. Klem, unpublished.
[35] H. Sakakibara, M. Noguchi, T. J. Thornton, H. Hirakawa, and T. Ikoma, Proceeedings of the 1993 IEDM, p. 411; and N. Tsukada, A. D. Wieck, and K. Ploog, Appl. Phys. Lett. **56**, 2527 (1990).

Intentionally Left Blank

DISTRIBUTION:

1	MS-0601	J. S. Nelson, 1113
1	MS-0601	J. L. Reno, 1113
1	MS-0603	P. E. Esherick, 1314
1	MS-0603	J. F. Klem, 1314
1	MS-0603	J. R. Wendt, 1314
1	MS-1415	W. B. Gauster, 1112
1	MS-1415	J. S. Moon, 1112
6	MS-1415	J. A. Simmons, 1112
1	MS-0188	LDRD Office, 4523
2	MS-0619	Review & Approval Desk, 12690 (for DOE/OSTI)
5	MS-0899	Technical Library, 4414
1	MS-9018	Central Technical Files, 8940-2